Lab on a Chip

ROYAL SOCIETY OF CHEMISTRY

CRITICAL REVIEW

View Article Online
View Journal | View Issue

Check for updates

Cite this: *Lab Chip*, 2025, **25**, 4252

Liquid transport strategies in wearable and implantable microfluidic systems

Qi Wang,[a] Yizhen Jia[a] and Jinghua Li *[ab]

An essential capability of lab-on-a-chip systems is the precise handling, management, and transport of fluids within microfluidic channels. However, conventional rigid pump-tube-valve systems are often incompatible with emerging wearable and implantable devices, which demand miniaturization, low power consumption, high level of integration, and biocompatibility to ensure reliable and safe operation in biological environments. In recent years, various microscale fluid management and transport strategies have been developed to address these challenges, enabling actively programmable control and significantly advancing the capabilities of bio-integrated electronics. This review summarizes key advances in design architectures, performance control, and integration strategies across four actuation modes: passive, mechanical, pressure-mediated, and electric field-driven mechanisms. Emphasis is placed on their respective advantages and limitations in key application scenarios such as sensing, drug delivery, and biofluid sampling. Finally, we outline potential future directions including device format, comfort level, user safety, and sustained operation, aiming to provide a strategic reference for the development of next-generation fluid management modules in soft bioelectronic systems.

Received 16th June 2025,
Accepted 29th July 2025

DOI: 10.1039/d5lc00593k

rsc.li/loc

Open Access Article. Published on 30 julio 2025. Downloaded on 23/02/2026 2:23:37.
This article is licensed under a Creative Commons Attribution-NonCommercial 3.0 Unported Licence.

Introduction

In microfluidic systems, liquid transport is fundamental to key functions such as liquid delivery, reaction control, and drug release.[1–3] The transport strategy directly determines the efficiency of fluid distribution, the precision of temporal regulation, and the interface compatibility between the device and biological tissue.[4,5] Conventional platforms typically rely on external pumps, valves, and rigid tubing to maintain flow control,[6] supporting synchronized actuation across multiple channels and precise manipulation of microscale volumes.[7,8] These systems, each with their own advantages and limitations, are widely implemented in various platforms for customized applications and in automated analytical instruments, where mature control infrastructures are already in place.[9,10]

For example, piezoelectric pumps provide precise flow control, fast response times, and compact form factors, but their rigidity, limited flow rates, and poor compatibility with flexible devices limit their integration in soft systems.[11] Electrostatic pumps offer low power consumption, simple structure, and fast actuation, but are sensitive to humidity, generate low output force, and often require high operating voltages.[12] Thermal pneumatic pumps offer simple fabrication and reliable operation, but suffer from slow response times, high power consumption, and heat generation that may cause user discomfort.[13] Electromagnetic pumps offer high flow rates, fast response, precise control, and good compatibility with integrated circuits, but they can be bulky, power-consuming, require magnetic materials, and may generate electromagnetic interference.[14] Additionally, all these pioneering implementations are obtrusive, and their feasibility for building practical bio-integrated electronics remains largely unexplored.

As microfluidic systems transition from traditional, rigid platforms to emerging applications in real-world physiological environments—particularly in skin-mounted and implantable devices,[1] the limitations of conventional pumping technologies become increasingly important. The mechanical rigidity, high power demands, and bulky hardware associated with piezoelectric, electrostatic, thermal pneumatic, and electromagnetic pumps hinder their integration into soft, deformable systems.[15,16] These shortcomings are especially problematic in wearable and implantable platforms, where devices must function reliably under stringent constraints such as limited space and power,[17,18] continuous mechanical deformation, and the need for long-term biocompatibility.[19] In such dynamic and sensitive settings, conventional flow control methods often fail to deliver programmable, stable fluid transport within the minimal footprint and energy budget required.

[a] *Department of Materials Science and Engineering, The Ohio State University, Columbus, OH 43210, USA. E-mail: li.11017@osu.edu*
[b] *Chronic Brain Injury Program, The Ohio State University, Columbus, OH 43210, USA*

This journal is © The Royal Society of Chemistry 2025

Open Access Article. Published on 30 julio 2025. Downloaded on 23/02/2026 2:23:37.
This article is licensed under a Creative Commons Attribution-NonCommercial 3.0 Unported Licence.

Furthermore, their sensitivity to motion and mechanical stress adds additional complexity, making them poorly suited for dynamic biological environments. These challenges highlight the need for fundamentally rethinking liquid transport strategies—shifting away from rigid, energy-intensive components toward solutions that are inherently soft, low-power, miniaturizable, and seamlessly compatible with flexible bioelectronic systems.

To address these limitations, researchers have developed a variety of novel fluid transport strategies tailored to the constraints of soft and flexible systems. While this review discusses liquid transport strategies relevant to both wearable and implantable microfluidic systems, the majority of current implementations remain focused on wearable or semi-implantable devices. This is primarily due to the greater technical challenges associated with fully implantable systems, including the need for long-term biocompatibility, reliable power supply, stable operation in enclosed environments, and minimal immune response. As a result, the literature—and accordingly our discussion—naturally emphasizes wearable formats. Nonetheless, many of the strategies reviewed here offer foundational capabilities that are highly promising for future translation into fully implantable platforms, provided these key engineering barriers can be addressed. Based on their actuation mechanisms, this review classifies existing strategies into four categories: passive, mechanically driven, pressure-mediated, and electric field-driven, with details described below (Fig. 1). These strategies span the full spectrum from passive to active control and reflect a broader design evolution from structure-involved actuation toward field-based control. Correspondingly, the driving media involved progress from solid structures to gases and ultimately to electric fields. Each category presents unique trade-offs in terms of power consumption, precision of control, flow rate/speed, and structural complexity, and exhibits distinct advantages and applicable scenarios.

Major categories of liquid transport strategies for bio-integrated electronics

Passive liquid transport strategies enable directional fluid flow without the need for external energy input, relying instead on interfacial wettability, surface energy gradients, or geometric barriers.[20,21] These systems eliminate the need for pumps, valves, or electronic components, resulting in structurally minimal designs that are well-suited for miniaturization and on-chip integration.[22] They are compatible with scalable manufacturing processes such as three-dimensional (3D) printing and photolithography.[23] Fluid manipulation is governed primarily by device geometry and surface functionalization, allowing broad material compatibility and facilitating the use of biocompatible substrates.[17] Furthermore, the absence of electromagnetic components imparts intrinsic electromagnetic silence, preventing interference with co-integrated electronic modules. These features make passive transport systems particularly attractive for wearable or implantable devices operating under stringent power and environmental constraints.[24] Nonetheless, because fluid actuation is predetermined by static structural and interfacial features, these systems generally lack tunability, such as flow rate modulation or pathway switching, thereby limiting their utility in complex workflows or multi-step analytical operations.[25] Additionally, passive transport performance is often susceptible to environmental variations—including humidity, surface fouling, and mechanical deformation—which can compromise long-term stability and reproducibility, posing challenges for deployment in dynamic physiological settings.[26]

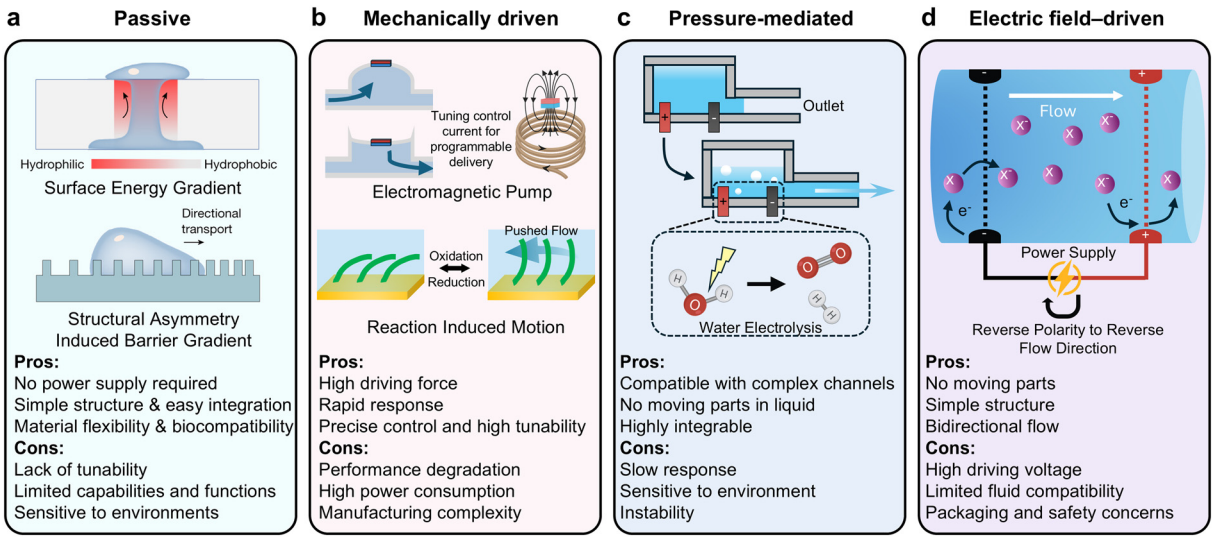

Fig. 1 Comparison of representative liquid transport strategies for wearable and implantable systems, highlighting typical actuation mechanisms and summaries of their respective advantages and limitations. Four categories are shown: (a) passive (reproduced from ref. 90 with permission from Springer Nature, 2023), (b) mechanically driven, (c) pressure-mediated (created with **https://BioRender.com**), and (d) electric field-driven.

Open Access Article. Published on 30 julio 2025. Downloaded on 23/02/2026 2:23:37. This article is licensed under a Creative Commons Attribution-NonCommercial 3.0 Unported Licence.

Mechanical actuation strategies—which can also be referred to as "responsive actuation mechanisms" in a broader sense—rely on the direct coupling between movable structures and fluid interfaces to enable active control of fluid transport, such as regulating flow direction or flow rate.[27,28] In this context, we define "mechanical" actuation as systems in which movable structures directly interact with the liquid to generate flow, regardless of the underlying energy source—be it magnetic, electrochemical, or thermal. The movable components can perform motions including rotation,[29] vibration,[30] or bending,[31,32] driven by mechanisms such as magnetic response, electro-induced deformation, or structural changes triggered by electrochemical reactions.[31] The strong mechanical coupling with the fluid endows the system with high driving force, rapid response, and precise control capabilities.[28] However, the integration of movable components increases structural complexity, making miniaturization and system integration more challenging and placing higher demands on fabrication precision.[33] When continuously exposed to liquid environments, these components are prone to performance degradation due to mechanical fatigue, material degradation, or contamination, thereby affecting the system's stability and lifespan.[34] In addition, mechanical actuation methods—such as magnetic actuation based on coil systems—typically involve high energy consumption, which may lead to localized heating and adversely impact material performance or biocompatibility in sensitive environments.[35]

Pressure-mediated strategies can be considered an extension of mechanical actuation, with gas serving as an intermediary in the energy transmission process. A common approach involves using movable components to alter the volume of a sealed chamber, thereby regulating internal pressure and indirectly driving liquid flow.[36] This design avoids direct contact between movable parts and the working fluid. Another representative method utilizes the density difference between liquids and gases—by electrolyzing water to generate gas, internal pressure increases and provides the necessary driving force.[37,38] Owing to the shapeless nature of gas, such systems are compatible with complex two-dimensional and even three-dimensional channel geometries, making them well suited for highly integrated designs.[39] However, the gas generation process *via* electrolysis is relatively slow, limiting its applicability in rapid or high-frequency operations.[37,38,40] Moreover, gas-mediated systems are sensitive to temperature fluctuations, material elasticity, and device deformation, which can lead to instability and reduced repeatability in long-term or dynamic applications.[41]

Electric field-driven strategies represent a broad category of mechanisms that, although all rely on externally applied electric fields, differ significantly in their underlying physics and fluid manipulation approaches. Common types include electroosmotic flow,[42] electrowetting on dielectric surfaces,[43] dielectrophoresis,[44,45] and electrohydrodynamics (EHD).[46–49] Electroosmotic flow is typically used for transporting continuous liquids within charged microchannels; electrowetting enables the manipulation of discrete droplets; and dielectrophoresis is mainly employed for positioning and controlling particles or droplets. In contrast, EHD induces fluid motion by applying a high electric field across insulating liquids, leading to the formation of space charges that experience Coulombic forces and, in turn, impart momentum to the surrounding fluid.[50,51] This mechanism, which operates through charge injection or interfacial polarization at the electrode–liquid interface, relies on a simple two-electrode configuration and contains no moving parts. Its structural simplicity, mechanical robustness, and compatibility with flexible and miniaturized platforms have made EHD pumping an increasingly attractive strategy for wearable and implantable fluidic systems.[52] Moreover, in symmetric electrode designs, the direction of flow can be reversed by simply switching the polarity of the applied voltage, enabling bidirectional control without additional mechanical components.[46–49,53] However, the applicability of EHD is limited by several factors. It is generally restricted to insulating liquids with low conductivity and high dielectric strength, making it incompatible with physiological buffers, ionic solutions, or other aqueous systems.[50] Additionally, EHD pumps typically require high driving voltages—often several hundred volts or more—which introduces challenges in power management, device safety, and electromagnetic compatibility, particularly in flexible, wearable, or implantable applications.[46–49]

Most of the literature discussed in this review focuses on microfluidic platforms for bio-integrated electronic devices. However, we have also included selected studies that explore unconventional fluid handling strategies based on unique mechanisms and promising performance characteristics.[31,54] While some of these approaches have not yet been applied in wearable or implantable scenarios, their inherent potential for future bio-integrated applications makes them worth mentioning. Together, these fluidic strategies represent the primary actuation paradigms for flexible microfluidic systems, spanning the spectrum from passive self-regulation to active, programmable control. This review provides an overview of recent advances in these strategies tailored for wearable and implantable platforms. Focusing on four representative categories, we systematically examine their working principles, device architectures, performance metrics, and application domains, highlighting their respective advantages and limitations. We further compare their integration compatibility, controllability, and biological applicability, aiming to offer a structured reference framework to guide the design and selection of liquid handling modules in next-generation soft bioelectronic systems.

Passive liquid transport enabled by interfacial and structural design

Passive liquid transport systems have attracted increasing attention in flexible and wearable devices due to their structural simplicity and capability of operating without

 This journal is © The Royal Society of Chemistry 2025

Open Access Article. Published on 30 julio 2025. Downloaded on 23/02/2026 2:23:37.
This article is licensed under a Creative Commons Attribution-NonCommercial 3.0 Unported Licence.

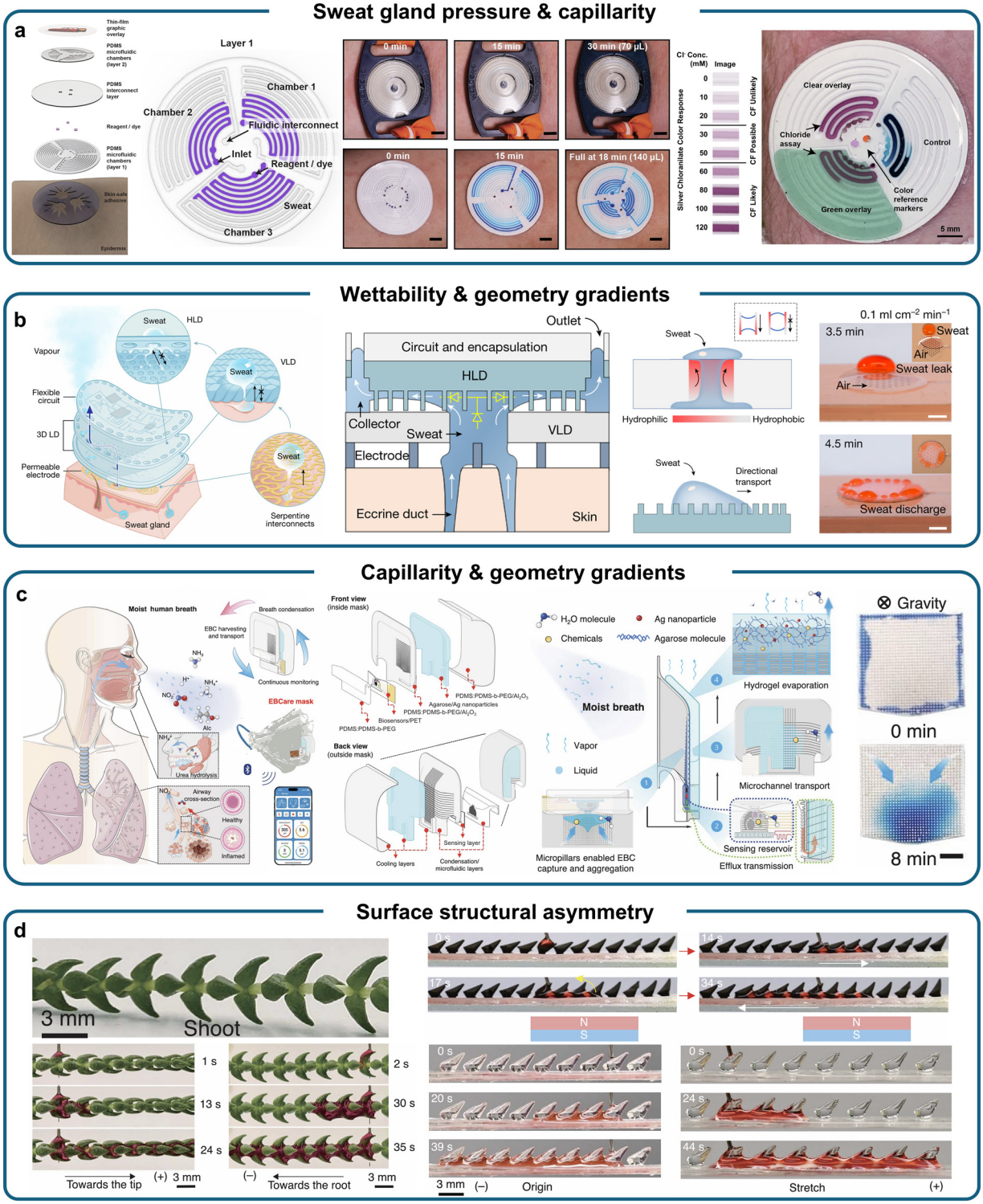

Fig. 2 Passive liquid transport enabled by interfacial and structural design. (a) A flexible microfluidic patch for passive sweat sampling and power-free chloride sensing.[81] Reproduced from ref. 81 with permission from the American Association for the Advancement of Science, 2021. (b) A 3D liquid diode enabling directional sweat removal through wettability and geometry gradients.[90] Reproduced from ref. 90 with permission from Springer Nature, 2023. (c) A smart mask platform for continuous exhaled breath condensate collection and *in situ* molecular analysis *via* geometry-driven capillary microfluidics.[70] Reproduced from ref. 70 with permission from the American Association for the Advancement of Science, 2024. (d) A bioinspired reconfigurable surface achieving unidirectional flow *via* structural asymmetry.[54] Reproduced from ref. 54 with permission from the American Association for the Advancement of Science, 2024.

Open Access Article. Published on 30 julio 2025. Downloaded on 23/02/2026 2:23:37. This article is licensed under a Creative Commons Attribution-NonCommercial 3.0 Unported Licence.

external energy input.[20,23] These systems rely on mechanisms such as capillary forces, wettability gradients, or geometric guidance to achieve spontaneous fluid transport in the absence of active driving.[5,55] Through surface engineering and structural design, researchers have developed a variety of passive microfluidic devices that enable directional guidance, distribution, retention, or mixing of liquids, providing critical support for integrated and low-power fluid handling and management platforms.

Among various applications, sweat collection represents a key research focus in passive transport systems. As a biofluid rich in electrolytes and metabolic byproducts, sweat offers real-time insights into an individual's health status,[56] electrolyte balance,[57] metabolic activity,[58] and disease risk.[59,60] Unlike conventional active sampling systems, current mainstream sweat collection platforms are primarily driven by endogenous pressure generated by eccrine sweat glands (typically around 70 kPa),[61] which propels sweat into microchannel structures adhered to the skin, enabling a completely passive, pump-free sampling process.[61–63] To enhance the efficiency and reliability of sweat capture under this endogenous driving mechanism, researchers have employed various auxiliary strategies, including sealed microchannels,[64–66] surface patterning for directional flow,[67] capillary-guided structures, and evaporation-assisted transport.[68] These systems have demonstrated significant progress in continuous sampling, evaporation control, contamination prevention, and integrated analysis capabilities.[61,69] While sweat has been widely explored in passive wearable microfluidics, similar principles have also been extended to other physiologically relevant fluids such as exhaled breath condensate,[70] tears,[71,72] urine,[73,74] blood,[75,76] and saliva.[77,78] Wearable platforms including absorbent patches,[61] bandages,[79] and diaper-based sensors[80] have demonstrated the ability to monitor these fluids in a passive, noninvasive, and continuous manner. These applications further highlight the versatility of passive liquid handling strategies in enabling biosensing across a broad range of biofluids and use scenarios. Fig. 2a illustrates a representative example: a flexible sweat patch capable of continuously collecting sweat and performing on-body ion analysis without the need for batteries, primarily designed for quantifying chloride levels in cystic fibrosis (CF) screening.[81] Structurally, the device is composed of a low-modulus polydimethylsiloxane (PDMS) that conforms to the skin and forms a tight seal. Internally, multiple serpentine microchannels (each with a volume of approximately 47 μL) direct sweat into terminal reservoirs. The channel geometry is optimized to match glandular secretion rates and prevent backflow, enabling a mean collection rate of approximately 7.8 μL min^{-1}. The fully enclosed design minimizes evaporation and external contamination, ensuring reliable sample capture. Upon reaching the terminal reservoirs, sweat reacts with a preloaded colorimetric reagent—silver chloranilate—to enable *in situ* chloride detection. This reagent forms a purple-red complex upon interaction with chloride ions, and the color intensity correlates with ion concentration. The reaction occurs spontaneously within five minutes, without requiring power, electronics, or external sensors. This integration demonstrates how passive liquid transport can be extended to drive autonomous biochemical analysis. To assess clinical performance, the system is benchmarked against the Macroduct sweat collection system (MSCS), a gold-standard device commonly used for CF diagnosis. A long-standing challenge for using MSCS is how to collect sufficient volume, especially in infants or individuals with low sweat rates. In a study involving 51 participants of various ages, the flexible patch collects an average volume of 73.6 ± 35.2 μL—significantly higher than that of MSCS (58.4 ± 24.1 μL)—and reports no quantity not sufficient (QNS) cases, compared to a 5.8% QNS rate with MSCS. Its improved adhesion and efficient fluid capture make it particularly well-suited for soft or low-perfusion skin areas.

Textile-based fluid transport platforms offer unique advantages for skin-interfaced systems due to their intrinsic porosity, breathability, and mechanical adaptability. Unlike elastomeric or plastic materials, woven or knitted fabrics provide a naturally interconnected capillary network that supports power-free sweat movement and moisture evaporation, while maintaining conformal skin contact.[82–84] These features make textiles particularly suitable for applications requiring prolonged skin wear, fluid sampling, and biosensing. Early studies demonstrated the use of multi-filament threads embedded in fabrics to construct yarn-based microfluidic channels for bioanalysis.[82] This concept evolved into textile total analysis systems by chemically modifying yarn surfaces and tailoring weave geometry to guide fluid transport.[83] More recently, stitched textile microfluidics have integrated hydrophilic threads into garments, enabling passive, stretch-tolerant sweat handling with high washability.[84] Janus fibers, wettability engineering, and capillary-assisted pumping further improve directional transport and retention under deformation.[85–87] A recent vertical textile microfluidic (VTM) platform exemplifies these advances by enabling on-garment sweat collection and biosignal readout through vertical wicking and interfacial pressure balancing.[88] These innovations establish the foundational strategies that support the development of complex textile-integrated fluidic systems. However, beyond sweat capture and sensing, wearable bioelectronics must also address the continuous accumulation of moisture at the device–skin interface, which can lead to signal degradation, material delamination, and user discomfort during prolonged wear.[64,89] To tackle this issue without relying on active components, a recently reported three-dimensional liquid diode (3D LD) structure (Fig. 2b) offers a fully passive solution, combining textile-based wettability gradients with microstructured fluidic paths to enable unidirectional sweat drainage and evaporation.[90] This system forms a multidirectional fluidic pathway with both vertical and horizontal transport capabilities, allowing sweat to follow a predefined path for directional transport and eventual discharge, without the need for pumps or electrical actuation. Specifically, the vertical liquid diode (VLD) utilizes plasma-treated textiles to

 This journal is © The Royal Society of Chemistry 2025

Open Access Article. Published on 30 julio 2025. Downloaded on 23/02/2026 2:23:37. This article is licensed under a Creative Commons Attribution-NonCommercial 3.0 Unported Licence.

establish a hydrophilic/hydrophobic gradient, enabling unidirectional sweat routing *via* interfacial energy differences. With optimized design parameters, a single VLD channel achieves a maximum flow rate of 1.4 mL min^{-1}, while the system-level transport rate reaches 11.6 mL cm^{-2} min^{-1}, approximately 4000 times higher than the human perspiration rate during mild exercise. The horizontal liquid diode (HLD) integrates a superhydrophilic poly(vinyl alcohol) (PVA)/SiO_2 composite coating onto PDMS micropillars arranged in a spacing-gradient array, forming geometric energy barriers that promote directional lateral spreading and discharge. The HLD maintains stable transport speeds exceeding 10 mm s^{-1} even under repeated mechanical deformation. The entire 3D LD construct is built as a multilayer modular system comprising a superhydrophobic supporting layer, selectively treated VLD pathways, and a gradient-structured HLD top layer, laminated *via* a flexible adhesive interface. This design achieves excellent breathability and fluid throughput while preserving structural integrity and sweat removal efficiency under continuous perspiration and complex deformation. The 3D LD system has been further validated in human subject studies, maintaining consistent sweat transport and mechanical integrity during extended wear and dynamic motion, without causing skin irritation or interface delamination. By continuously evacuating sweat from critical interfaces, it ensures a dry, breathable microenvironment, which is essential for preserving both signal quality and material adhesion. Building upon this passive drainage capability, the 3D LD architecture has been integrated into multiple wearable platforms, including electrophysiological monitoring and environmental sensing. In both applications, the 3D LD layer functions as a moisture-barrier substrate, supporting reliable operation of underlying components while adapting to dynamic physiological and environmental conditions. These findings highlight the importance of advanced passive fluid management strategies in enabling stable, long-term performance for diverse wearable technologies.

In addition to sweat collection and transport strategies, increasing attention has recently been directed toward exhaled biofluids.[91–93] Exhaled breath contains not only rich physical information but also a variety of biochemical markers, including volatile organic compounds, inorganic small molecules (such as NO and NH_3), water-soluble non-volatile species (such as nitrite and ammonium ions), metabolic products (such as ethanol), and components related to inflammation or infection.[91–93] These constituents are often dissolved in microdroplets formed during exhalation and subsequently condensed into exhaled breath condensate (EBC), a noninvasive, dynamic, and information-rich liquid sample.[91,94,95] As a result, realizing efficient condensation, collection, transport, and real-time analysis of EBC on wearable platforms emerges as a key direction for advancing liquid handling strategies.[96,97] Expanding the liquid routing and collection capabilities of microfluidics beyond sweat collection highlights the broader significance of this technology in quantitative analysis. One representative study proposes the EBCare system—an intelligent mask platform that integrates condensation, collection, transport, and analysis, aiming to enable *in situ*, continuous monitoring of key health biomarkers in EBC (Fig. 2c).[70] The system employs a passive "tandem cooling" mechanism that combines hydrogel-based evaporative cooling and a radiative cooling coating, enabling efficient condensation of exhaled vapor under various environmental conditions. It supports all-day operation both indoors and outdoors, achieving EBC collection rates of up to 5 mL min^{-1}, which ensures a stable liquid input for downstream processing. Once condensation occurs, a built-in microfluidic transport module activates to drive liquid flow passively using a geometry-enabled mechanism. This module incorporates a micropillar array with dual gradients in height and density, establishing a sustained capillary pressure difference between the condensation zone and the sensing chamber. This design enables spontaneous, directional transport of EBC along a predefined path without the need for gravity or external actuation. To ensure long-term wettability and transport reliability, the structural material is modified with 1 wt% PDMS-*b*-PEG copolymer, reducing the water contact angle to approximately 15.5°. Unlike plasma-treated PDMS, this surface maintains its hydrophilicity for up to one month, supporting stable capillary transport throughout prolonged use. Experimental validation demonstrates that the microfluidic structure operates reliably under various postures. Even in a supine position, EBC is transported from the condensation surface to the sensing chamber within 5 minutes, significantly outperforming flat or non-structured hydrophilic controls. This confirms the system's strong directional transport capability and posture independence. After reaching the integrated sensing chamber, the collected EBC is analyzed *in situ via* a multiplexed electrochemical sensor array capable of detecting pH, NH_4^+, NO_2^-, and ethanol, among other biomarkers relevant to respiratory or metabolic status. The sensing module is seamlessly integrated with the microfluidic path, allowing automatic sampling and real-time monitoring. Post-analysis, the liquid is directed through microchannels to the outer hydrogel layer, where it refreshes the evaporative cooling system. This forms a closed-loop liquid management cycle. The entire system operates continuously for over 7 hours without external pumps or a power supply and effectively resists interference from saliva contamination, offering a stable and reliable solution for wearable molecular breath analysis. Beyond engineered systems developed for wearable biofluid management, certain passive liquid control mechanisms are also inspired by natural microstructures that have evolved to regulate fluid transport without external energy input.[98,99] The study shown in Fig. 2d takes inspiration from the asymmetric epidermal structures found on the stems of *Crassula muscosa* and develops a flexible microstructured platform capable of unidirectional liquid transport and programmable flow control under passive conditions.[54] By constructing an array of wedge-shaped cavities with re-entrant geometries, the system enables spontaneous, one-way fluid flow solely by modulating the stability of liquid menisci through surface topology. Structurally, the platform is fabricated from Ecoflex elastomer

Open Access Article. Published on 30 julio 2025. Downloaded on 23/02/2026 2:23:37.
This article is licensed under a Creative Commons Attribution-NonCommercial 3.0 Unported Licence.

embedded with Neodymium–iron–boron (NdFeB) magnetic microparticles. A single-step replication process using a rigid mold is employed to generate the biomimetic surface textures and impart magnetic responsiveness. This manufacturing method is simple, scalable, and compatible with large-area flexible integration. On this basis, a structural reconfiguration mechanism is further introduced to enable dynamic regulation of fluid pathways. The system incorporates flexible fin-shaped transport units that respond to both mechanical stretching and magnetic stimuli. By adjusting inter-channel spacing and surface contact characteristics, the structure allows for active switching and reversal of fluid direction. Under tensile strain, the increased spacing alters the meniscus configuration, triggering flow reversal; under magnetic stimulation, the embedded particles cause directional deflection of the fins, enabling remote, reversible routing of droplets through the channel network. Without the need for electrodes or pumps, the platform forms a highly coupled "structure deformation-fluid response" loop for programmable passive control. Furthermore, multiple responsive units can be assembled into a two-dimensional array, forming a programmable liquid manipulation network. By selectively applying magnetic fields or localized strain, individual channels can be toggled between open and closed states, enabling droplet splitting, mixing, redirection, and path reconfiguration. Functionally, the system mimics "liquid logic gate" behavior. While maintaining a passive operating mode, it achieves control complexity approaching that of active systems, demonstrating the powerful potential of bioinspired architectures for energy-efficient, reconfigurable fluidic control.

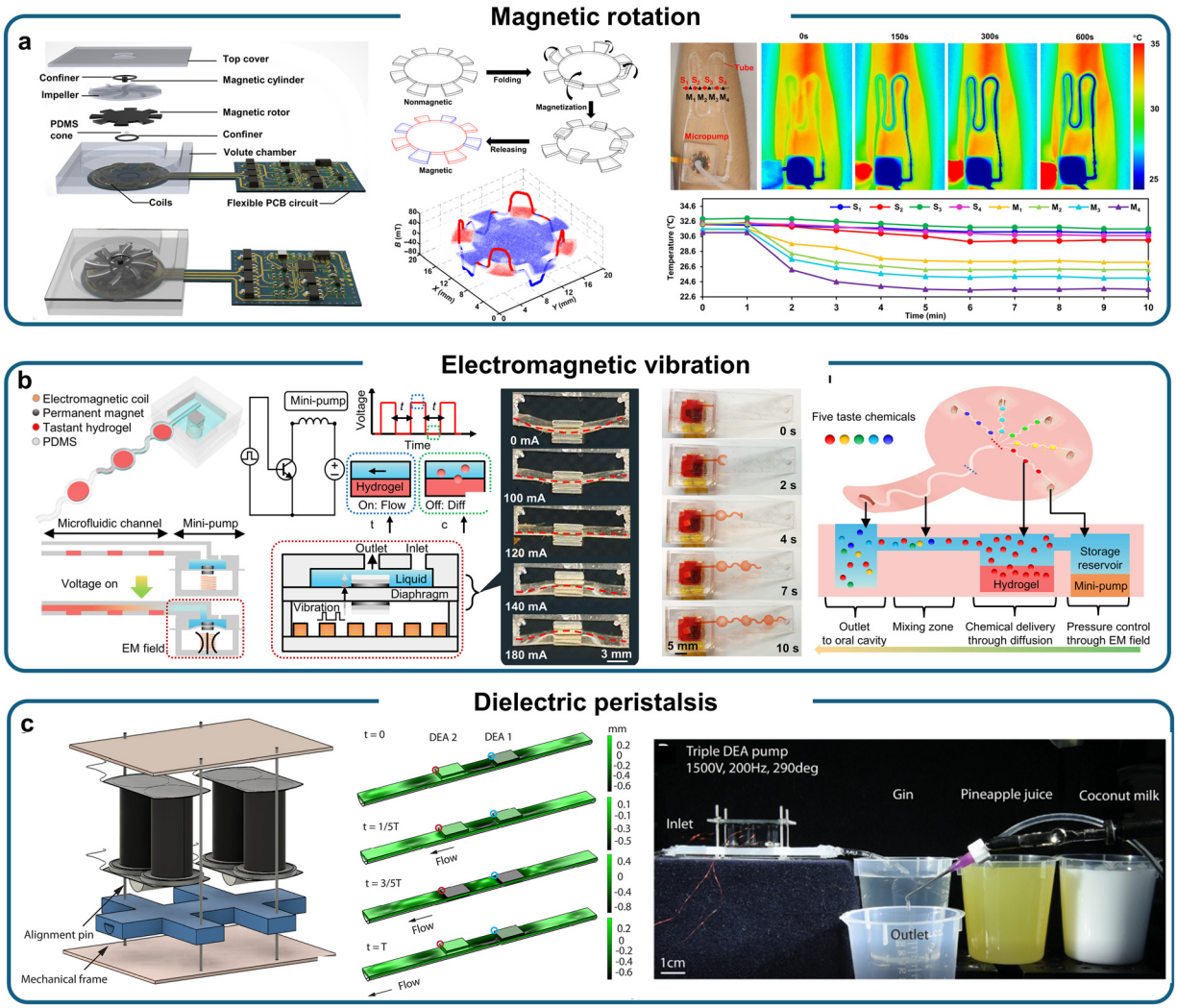

Fig. 3 Mechanically actuated strategies for active liquid transport in microfluidic systems. (a) A soft magnetically levitated centrifugal pump for high-throughput, contactless flow control.[29] Reproduced from ref. 29 with permission from the American Association for the Advancement of Science, 2021. (b) An electromagnetic diaphragm micropump for tunable taste delivery in wearable interfaces.[30] Reproduced from ref. 30 with permission from the American Association for the Advancement of Science, 2025. (c) A dielectric elastomer-based peristaltic pump for fast, bidirectional flow in soft systems.[109] Reproduced from ref. 109 with permission from the American Association for the Advancement of Science, 2023.

This journal is © The Royal Society of Chemistry 2025

Open Access Article. Published on 30 julio 2025. Downloaded on 23/02/2026 2:23:37.
This article is licensed under a Creative Commons Attribution-NonCommercial 3.0 Unported Licence.

Mechanical actuation strategies for liquid transport

While passive transport strategies offer advantages such as structural simplicity and no energy consumption, they face limitations in flow rate modulation, capability of switching directions, and precise timing control.[100–102] To achieve more advanced, precise, and controllable fluid manipulation, researchers have developed mechanically driven strategies centered on structural motion. These systems employ movable components whose deformation or displacement directly couples with the liquid interface, enabling stable and controllable fluid propulsion. Common actuation mechanisms include magnetically driven rotors[29] or vibrating elements,[30,103] electrochemically induced asymmetric expansion and bending,[31] and strain responses from dielectric elastomer actuators under electric fields.[104]

In a representative study (Fig. 3a), a flexible and miniaturized magnetically driven centrifugal pump system is demonstrated.[29] The system is actuated *via* a contactless rotating magnetic field and maintains stable operation under various mechanical deformations, including tilting, bending, and compression, making it well-suited for wearable or implantable applications in fluid transport and thermal regulation. In this design, the rotor is fabricated *via* mold casting using a composite of Ecoflex elastomer embedded with NdFeB magnetic microparticles. This material provides both high magnetic responsiveness and mechanical compliance, enabling low-friction, self-aligned rotation on the liquid surface. The pump body is constructed from PDMS through soft lithography and multilayer encapsulation, forming a spiral microfluidic channel precisely aligned with the rotor's motion to achieve directional fluid transport. Driven by an external rotating magnetic field, the rotor achieves a maximum flow rate of 30.6 mL min^{-1} under zero back pressure. The flow rate can be precisely tuned by adjusting the rotation speed of the magnetic field (0–1000 rpm), allowing programmable control over fluid delivery within the range of 0 to 30.6 mL min^{-1} in real time. When two pumps are connected in series, the pressure head increases to 58.7 mm, while a parallel configuration raises the flow rate to 33.7 mL min^{-1}, demonstrating the system's modular scalability. The pump accommodates fluids with a wide range of viscosities (1–6 cP), including water, blood, glucose solutions, and fat emulsions. Under high-viscosity conditions (*e.g.*, fat emulsion), the device still maintains a flow rate of 15.5 mL min^{-1}, indicating strong fluidic compatibility. Power consumption is measured at 4.1 W at 1000 rpm and 1.15 W at 500 rpm. Infrared thermography confirms that the surface temperature stabilizes at 34 °C after 30 minutes of continuous operation, which is below body temperature and suitable for prolonged skin contact. Owing to its magnetically levitated structure and soft materials, the device exhibits excellent mechanical compliance and operational stability. It can initiate rotation at tilt angles up to 180° (low speed) and sustain high-speed rotation (1000 rpm) at tilt angles up to 120°. It also remains functional under bending (minimum radius of ~60 mm), compression, and mild stretching, with negligible performance degradation. The absence of physical contact between the rotor and the pump chamber allows stable operation even under structural deformation. In practical applications, the pump is capable of not only continuous microfluidic delivery but also localized active cooling when coupled with thermally conductive liquids. Infrared thermal imaging demonstrates precise temperature modulation, highlighting its potential for wearable thermal management, personal cooling, and therapeutic heating platforms.

Beyond biomedical and thermal regulation applications, microfluidic systems have also been explored for immersive human–computer interaction, particularly in taste stimulation for augmented and virtual reality (AR/VR). These interfaces demand precise, low-volume, multichannel fluid control to simulate diverse taste sensations in real time. For example, recent studies have demonstrated portable gustation platforms that employ miniature, multi-taste microfluidic pumps for VR/AR/mixed reality (MR) settings, enabling independently tunable taste channels across compact, wearable formats.[105] Other systems have introduced transparent film-based displays that synchronize tastant spray with licking gestures to simulate "lickable" screens,[106] while sensor-driven taste replicators chemically analyze real food and reconstitute its flavor *via* on-demand microfluidic mixing.[107] Additionally, non-contact delivery methods—such as focused ultrasound-induced atomization—have been explored to release real food-derived liquid flavors without physical nozzles.[108] Collectively, these studies underscore the growing demand for soft, programmable, and concentration-tunable liquid handling systems. Building upon these needs, Fig. 3b illustrates a vibration-driven, electromagnetically actuated flexible micropump specifically developed to address the challenges of taste delivery in AR/VR environments.[30] This device integrates a PDMS microchamber with a magnetically responsive diaphragm to enable precise control of fluid transport and solute concentration on a flexible platform. The system uses an elastic PDMS membrane as a vibrating element, with a small NdFeB magnet embedded at its center to form a magnetic diaphragm. A copper coil positioned beneath acts as the electromagnetic actuator. When an alternating current is applied, the diaphragm undergoes vertical oscillations that cyclically deform the chamber volume, thereby driving fluid flow. Experimental results demonstrate that at a driving current of 180 mA, each channel can deliver 40 μL of liquid within 10 seconds, indicating excellent flow control performance. The flow rate is regulated by modulating the actuation parameters such as frequency, duty cycle, and current, allowing precise control over fluid delivery within a range of 0 to 348 μL min^{-1}. Solid-state taste compounds (such as sweeteners or acids) are preloaded into the pump channels in the form of tastant-infused hydrogels. As the liquid flows through these regions, it dissolves the solutes to form the target solution. By tuning the frequency, duty cycle,

Open Access Article. Published on 30 julio 2025. Downloaded on 23/02/2026 2:23:37. This article is licensed under a Creative Commons Attribution-NonCommercial 3.0 Unported Licence.

and pulse width of the electromagnetic input, the system precisely controls the fluid's residence time and velocity, thereby modulating the extent of solute dissolution and enabling programmable output concentration. Without requiring sensors or feedback circuits, the system achieves concentration-tunable delivery solely based on fluid–solid contact time. For instance, the output concentration of an acidic tastant (H^+) can be reliably adjusted within the range of 0.195–8.738 mM. At the system level, a flexible five-channel mixing module is implemented, with each channel corresponding to one of the five basic tastes: sweet, salty, sour, bitter, and umami. Each channel operates independently in terms of activation sequence and contact timing. After dissolution, the fluids converge in a central mixing zone, enabling synchronized and concentration-tunable multi-taste output. This system introduces a novel interface for human–machine interaction and multimodal sensory feedback, with promising applications in wearable and perception-enhancing technologies. Within the category of mechanically driven strategies, dielectric elastomer actuators (DEAs) offer an efficient and flexible approach to fluid pumping. By applying a high voltage across a soft dielectric elastomer membrane, DEAs generate electric-field-induced axial compression and lateral expansion, producing periodic deformation that drives fluid motion. Compared to other actuation mechanisms, DEAs feature high power density, rapid response, lightweight and soft construction, and strong programmability, making them especially suitable for applications requiring precise control of flow rate, pressure, or direction. Fig. 3c presents a compact DEA-based soft peristaltic pump designed to provide continuous fluid propulsion and integrated actuation for soft robotic systems.[109] Multiple DEA units are distributed along the surface of a soft channel to mimic peristaltic motion. The actuators are fabricated using Elastosil P7670 silicone in a multilayer rolled configuration, each with an added tip mass to tune the resonant frequency to 200 Hz for stable operation. The fluidic channel is made of Dragon skin 20 elastomer and features a concave cross-section (1 mm × 4 mm) that reduces backflow while conforming to the curvature of the DEA contact region. By tuning the driving voltage, phase offset, and spatial arrangement of the DEAs, the system achieves programmable and optimized pumping performance, enabling precise control over both flow rate and direction in real time within a range of −28 to +28 mL min^{-1}. Under a three-unit configuration, the pump reaches a flow rate of approximately 39 mL min^{-1} and sustains a back pressure up to 12.5 kPa when operated at +1680 V with a phase offset around 290°. It exhibits fast dynamic response, with actuation onset within 0.1 seconds, and functions reliably across a wide range of fluid viscosities. Bidirectional flow and pressure modulation are also supported through electrical control alone. Finite element simulations confirm that this phase setting maximizes pumping efficiency, with system behavior governed primarily by elastohydrodynamic coupling between the DEA and the channel wall. In practical demonstrations, the DEA-based pump successfully powered a finger-like bellows actuator and a wearable haptic feedback device, enabling closed-loop control of bending angle. Moreover, by adjusting actuation parameters, the system achieved selective routing and regulation of complex fluidic pathways under varying pressure conditions, highlighting its versatility as a power and control platform for soft robotic applications in fields such as food processing, biomedical systems, and human–machine interfaces.

Pressure-driven strategies for liquid transport

As an extension of mechanical actuation strategies, pressure-mediated approaches introduce gas as a medium in energy transmission. Due to the compressibility and shapeless nature of gases, external force applied at one end can be effectively transmitted over a distance, thereby avoiding direct contact between moving components and the working fluid while overcoming constraints imposed by channel geometry.[6,110,111] By generating gas *in situ* through water electrolysis within a sealed chamber, fluid flow can be driven directly or indirectly *via* an elastic membrane.[38,112,113] This enables miniaturization and high integration, making such systems particularly well-suited for stable fluid transport in microchannels with complex geometries.

A representative example employs a heterogeneous dielectric elastomer actuator (H-DEA) to dynamically regulate the internal pressure of a sealed elastomeric chamber. As shown in Fig. 4a, the fully soft pump operates using an H-DEA composed of multiple layers of high-performance dielectric elastomer (PHDE), laminated with a thin PDMS film that functions as both an electrical insulator and a fluid barrier.[114] Upon electrical activation, the H-DEA undergoes in-plane expansion, which deforms the membrane and increases the chamber volume. PHDE enables large actuation strain and high energy density, while PDMS provides dielectric safety and chemical stability. The entire device consists only of elastomeric materials without rigid supports, which allows stable operation during bending, stretching, or twisting. This configuration is well-suited for applications in wearable systems and soft robotics. The pump uses a diaphragm-based mechanism together with two check valves to ensure unidirectional fluid flow. In the resting state, the chamber contains a preloaded volume of liquid that generates an initial pressure of approximately 1200 Pa, causing the membrane to arch outward. When a high-voltage square wave (up to +1.8 kV) is applied, the H-DEA expands and increases the chamber volume, which lowers the internal pressure. This pressure drop opens the inlet valve and draws fluid into the chamber. When the voltage is removed, the H-DEA returns to its original shape, reducing the volume and increasing the internal pressure. As a result, the outlet valve opens and the fluid is expelled. Repeating this actuation cycle at an optimized frequency of 7 Hz enables continuous and directional fluid transport. The flow rate is tunable through electrical and mechanical parameters, such as voltage,

 This journal is © The Royal Society of Chemistry 2025

Open Access Article. Published on 30 julio 2025. Downloaded on 23/02/2026 2:23:37.
This article is licensed under a Creative Commons Attribution-NonCommercial 3.0 Unported Licence.

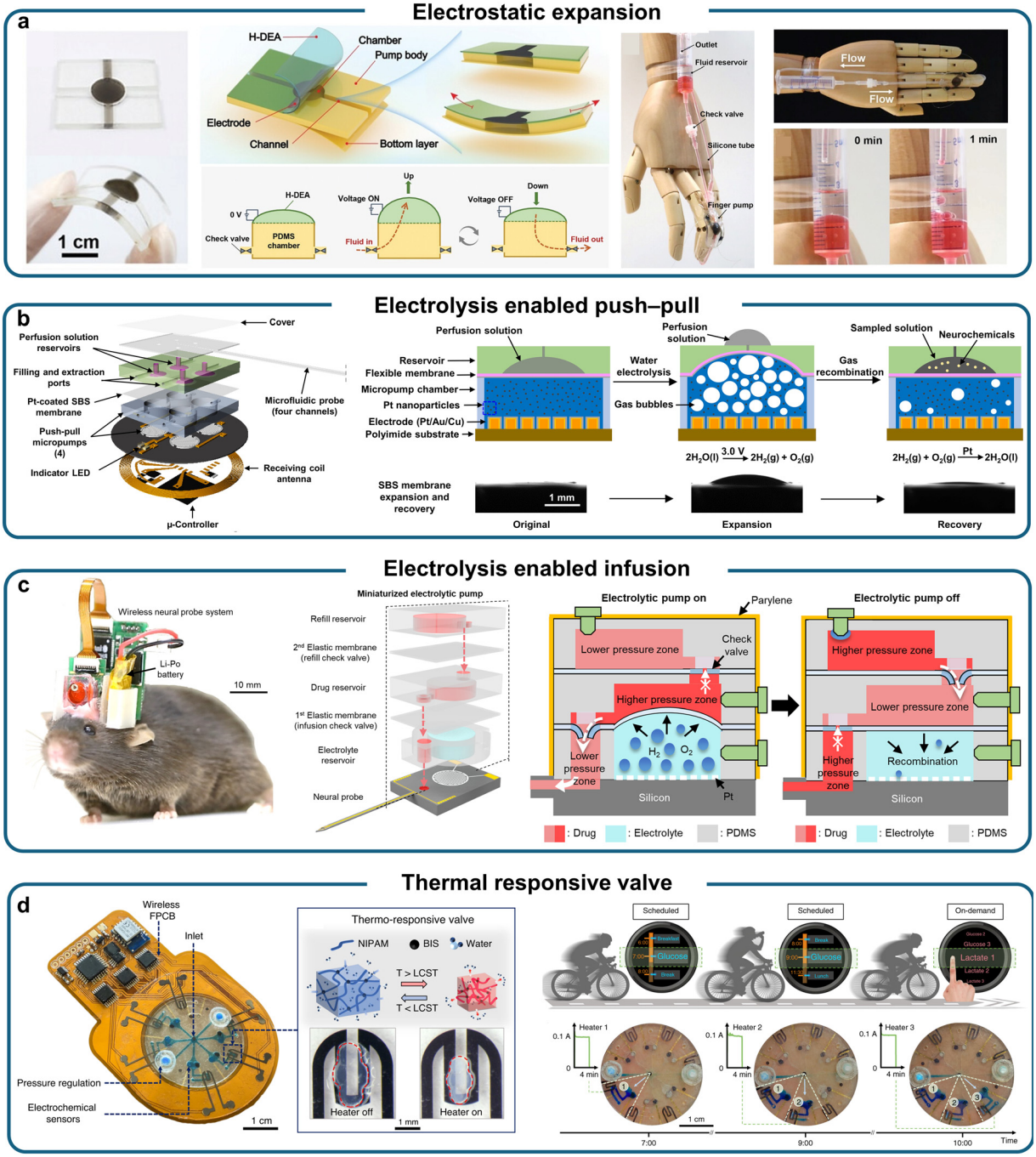

Fig. 4 Pressure-driven strategies for liquid transport in wearable and implantable microfluidic systems. (a) A stretchable dielectric elastomer pump enabling directional flow control in wearable and deformable platforms.[114] Reproduced from ref. 114 with permission from Wiley-VCH, 2024. (b) A battery-free, electrolysis-driven push-pull microsystem for reversible neurochemical sampling in freely moving animals.[37] Reproduced from ref. 37 with permission from the American Association for the Advancement of Science, 2022. (c) A wireless neural interface integrating electrolytic pumping for concurrent drug delivery and electrophysiological recording.[38] Reproduced from ref. 38 with permission from Springer Nature, 2022. (d) A thermoresponsive hydrogel valve array enabling programmable sweat sampling and biochemical analysis in epidermal systems.[15] Reproduced from ref. 15 with permission from Springer Nature, 2020.

frequency, membrane area, and the number of PHDE layers, allowing customized performance for specific application needs within a range of 0 to 3.25 mL min^{-1}. The performance of the pump depends on several factors, including the driving voltage, actuation frequency, membrane area, and the number of PHDE layers. Under optimized conditions, the pump delivers a maximum flow rate of 3.25 mL min^{-1} and a blocked outlet pressure of 2.75 kPa, while the power consumption is only 0.21 W. The total mass of the device remains below 1 gram, which reflects its high energy

Open Access Article. Published on 30 julio 2025. Downloaded on 23/02/2026 2:23:37.
This article is licensed under a Creative Commons Attribution-NonCommercial 3.0 Unported Licence.

efficiency and potential for integration into compact systems. System-level validation involves integrating the pump into a closed-loop fluidic circuit on a soft robotic finger. Even under bending deformation up to 70 degrees, the pump maintains continuous dye solution delivery to the fingertip, which demonstrates high adaptability in flexible environments. In addition, structural parameters such as membrane diameter, actuation area, and PHDE layer count can be customized. Connecting multiple pumps in parallel or series further expands flow and pressure output, enabling the platform to support complex fluidic control in soft, wearable, and miniaturized systems.

Compared to conventional fluidic actuation systems that rely on rigid mechanical components, gas-regulated pressure-driven strategies offer a promising path toward non-mechanical microfluidic control. In recent years, implantable drug delivery systems have advanced significantly, offering site-specific, programmable, and minimally invasive therapeutic strategies for chronic conditions and neuromodulation. A variety of actuation mechanisms and architectures have been demonstrated, including soft wireless implants for seizure intervention that respond to physiological triggers,[115] magnetically refillable peritoneal pumps that avoid transcutaneous refilling,[116] and electrochemically triggered bioresorbable reservoirs for single-use drug release.[117] Other innovations have combined mechanical actuation with structural dynamics to overcome fibrotic encapsulation and improve delivery efficiency over time,[118] while multifunctional neuropharmacological probes have integrated optofluidics and electrophysiology for behavioral modulation.[119] These studies highlight a growing need for compact, wireless, and energy-efficient systems capable of reliable operation in dynamic *in vivo* environments. Among various approaches, pressure-driven actuation *via in situ* gas generation has emerged as a promising solution, due to its compatibility with hermetically sealed, miniaturized, and fully implantable architectures.

By generating gas *via in situ* water electrolysis and inducing reversible deformation of a flexible membrane, fluid delivery and retrieval can be achieved without moving mechanical parts.[112] This approach not only simplifies structural design and enhances flexibility and hermetic sealing, but also enables precise, programmable fluid handling *via* electrical signals.[120] These features make the strategy well-suited for applications requiring wireless operation, valve-free flow control, and highly integrated miniaturized systems, particularly in bioimplants. Fig. 4b presents a wireless, programmable push–pull microsystem designed for neurochemical sampling.[37] The system consists of four miniaturized push–pull pumps, a flexible microfluidic probe, refillable fluid reservoirs, and a wireless power and control module. With a total weight of approximately 0.2 g, the device is lightweight and compact, suitable for implantation in freely moving animals for *in vivo* infusion and sampling. Its core actuation relies on electrolysis-driven gas generation: upon applying a voltage, gas is produced at the electrode interface, inflating a flexible membrane to drive fluid injection; subsequent gas recombination to form water —catalyzed by platinum nanoparticles—causes the membrane to relax and enables fluid retrieval into the reservoir, thus establishing a fully reversible push–pull cycle. To improve pumping efficiency and ensure long-term functionality, the system integrates platinum-coated interdigitated gold electrodes, an electrolyte composed of 50 mM NaOH with Nafion-coated platinum nanoparticles (PtNPs), and a stretchable styrene–butadiene–styrene (SBS) membrane coated with a 5-nm-thick platinum layer. This ultrathin Pt layer plays a critical role: as a high-efficiency catalyst, it significantly accelerates the recombination of hydrogen and oxygen gas bubbles on the membrane surface, facilitating rapid membrane recovery and reducing residual gas accumulation. Experimental results show that Pt-coated membranes yield gas recombination efficiencies exceeding 97%, greatly enhancing the speed, reliability, and reusability of the push–pull operation. The 5 nm thickness is optimized to retain high catalytic activity while preserving the membrane's mechanical compliance and elasticity for long-term cyclic actuation. Fluid delivery and sampling are achieved through a soft PDMS microfluidic probe containing four microchannels (10 μm × 10 μm each) with a total thickness of ~150 μm, enabling cellular-scale spatial resolution. The electronics module includes a low-power microcontroller, an indicator LED, and a 13.56 MHz receiving coil, allowing for wireless energy harvesting and independent pump control. Under optimized operating conditions (+3.0 V driving voltage, 40 mg ml^{-1} PtNP concentration), each 0.5 μL fluid injection takes 10–15 s, followed by complete retrieval within ~35 s. The flow rate and timing can be tuned by adjusting the applied voltage and PtNP concentration, enabling programmable and repeatable fluid handling without mechanical valves, with injection rates ranging from approximately 2 to 3 μL min^{-1} under optimized conditions. Both injection and collection efficiencies exceed 90%, with droplet volume variation under 10.5% across three repeated cycles, indicating excellent reproducibility and operational stability. *In vitro* testing confirms high recovery rates for potassium ions, dopamine, and neuropeptide Y (NPY), with particularly superior performance for large-molecule neuropeptides compared to conventional microdialysis. *In vivo* experiments further demonstrate that the device can dynamically capture NPY release upon pharmacological stimulation without altering animal behavior, highlighting its strong potential for high-resolution neurochemical monitoring in freely moving subjects.

Using a similar design, a number of pioneering studies have leveraged this concept for controlled drug delivery *in vivo*.[121–124] As an example, building upon this foundation, integrating an electrolytic pump-based controllable fluid delivery system with a neural probe enables wireless, miniaturized *in vivo* drug administration combined with neural signal recording. Fig. 4c presents such a probe incorporating a miniaturized electrolytic pump, the core

 This journal is © The Royal Society of Chemistry 2025

Open Access Article. Published on 30 julio 2025. Downloaded on 23/02/2026 2:23:37.
This article is licensed under a Creative Commons Attribution-NonCommercial 3.0 Unported Licence.

structure of which consists of multilayer PDMS housing and parallel microfluidic channels.[38] The pump includes separate reservoirs for electrolyte, drug, and refill solution, interconnected *via* elastic membranes and micro check valves to form a sealed fluidic circuit. Platinum black (Pt black) electrodes embedded in the pump electrolyze PBS under a +3.3 V driving voltage to generate gas, which recombines into water under the catalysis of Pt black and a Nafion coating, deflecting the membrane and driving drug infusion. After electrolysis stops, the recombined gases reduce internal pressure, allowing the membrane to return and passively draw drug from the refill reservoir, thus refilling the drug chamber. The probe shank, 6 mm in length, integrates ten 12 μm-high microchannels for low-pressure, high-efficiency fluid delivery. At the distal end, 16 Pt black microelectrodes enable simultaneous neural signal acquisition. The system achieves an average pumping rate tunable from 0.31 to 1.15 μL min^{-1} by adjusting the actuation cycle (*e.g.* 10 s, 30 s, 60 s), enabling programmable and reproducible drug delivery. With three activation cycles, approximately 300 nL of fluid can be delivered per injection. The infused volume shows a strong linear relationship with the number of activation cycles (R^2 = 0.94), and the system remains stable over five days of continuous operation without clogging or performance degradation. This system has been validated for use in neural modulation experiments in freely moving mice, offering wireless, programmable drug delivery alongside real-time electrophysiological recording. By implanting the probe into the substantia nigra or lateral hypothalamus and injecting bicuculline or muscimol, researchers induced behavioral changes such as circling or feeding suppression, while simultaneously monitoring neural firing patterns in target brain regions. Moreover, in a dual-mouse food competition assay, the system enabled real-time tracking of drug-induced changes in social behavior and corresponding neural activity, demonstrating its potential for investigating complex behavior-brain function interactions. In addition to active pressure-driven fluid transport strategies, passive pressure-regulated fluid management represents an alternative design approach. Instead of directly supplying energy to modulate chamber pressure for fluid propulsion, this strategy indirectly controls flow by regulating the open or closed state of microfluidic valves that modulate gas pathways. When the valve is closed, internally generated pressure (*e.g.*, from sweat secretion) is unable to drive further liquid movement, thereby achieving effective inhibition of flow.[125] This method preserves system flexibility and hermeticity while simplifying structural complexity, offering high integration potential and operational stability.[126,127] Fig. 4d presents a representative study in this category, which involves a wearable, programmable epidermal microfluidic valving system for controlled sweat sampling, routing, and compartmentalization.[15] The core of the system comprises multiple individually addressable thermoresponsive hydrogel valves based on poly(*N*-isopropylacrylamide) (PNIPAM). PNIPAM exhibits a reversible volume phase transition: it swells and blocks fluid flow below its lower critical solution temperature (~45 °C), and contracts to reopen the channel when heated above this threshold. By integrating microheater arrays onto a flexible substrate, precise thermal activation of each valve is achieved. Under activation, the PNIPAM hydrogel undergoes approximately 40% volume shrinkage, with a standalone response time below 20 s, and ~30–40 s when embedded in microchannels. To enhance switching speed and sealing efficiency, the hydrogel is patterned into circular structures approximately 1.2 mm in diameter. To address pressure buildup from continuous sweat secretion, the system incorporates a pressure release mechanism inspired by an electro-hydraulic analogy, stabilizing internal operating pressure between 10 and 200 mmHg and preventing structural failure. In the closed state, fluid flow is completely blocked; upon activation, fluid resumes flowing under a constant 15 mmHg pressure. The device withstands up to ~300 mmHg without leakage, enabling robust operation under physiological pressures. The platform integrates a flexible circuit for multichannel valve actuation and signal acquisition, with wireless communication to external smart devices *via* Bluetooth. *In vitro* tests demonstrated stable valve performance over a 6-hour period, and reliable switching under 5 Hz mechanical vibrations, indicating excellent mechanical robustness. In on-body experiments, the system was mounted on the subject's back and successfully activated different valves at predefined timepoints during physical activity to collect sweat into isolated compartments. Integrated electrochemical sensors enabled real-time analysis of glucose and lactate concentrations, while eliminating interference from flow rate variations. For example, under continuous flow at 5 μL min^{-1}, the estimated concentration of a 200 μM glucose sample was overestimated by 114%; in contrast, using the valve-gated "sample-hold-analyze" mode, the measurement closely matched the actual concentration, with an error below 5%. This study demonstrates the feasibility of passive valve-regulated liquid handling for wearable applications and provides a reliable solution for multi-chamber, time-resolved biomarker monitoring.

Electric field-driven strategies for microfluidic transport

Compared with conventional actuation methods that rely on solid or gas media to transfer kinetic energy, electric field-driven strategies enable contactless liquid transport by directly manipulating the internal charge distribution within the fluid for directional movement.[47,128] Among these, EHD pumps represent a key implementation.[128] They inject unipolar charges into insulating liquids, forming space charge regions under an applied electric field.[129] These free charges migrate under Coulomb forces and transfer momentum to electrically neutral molecules,[130] resulting in bulk fluid flow at the system level.[47,52,131]

EHD pumps operate without mechanically movable parts, feature simple structures, and are scalable in size. These

Open Access Article. Published on 30 julio 2025. Downloaded on 23/02/2026 2:23:37.
This article is licensed under a Creative Commons Attribution-NonCommercial 3.0 Unported Licence.

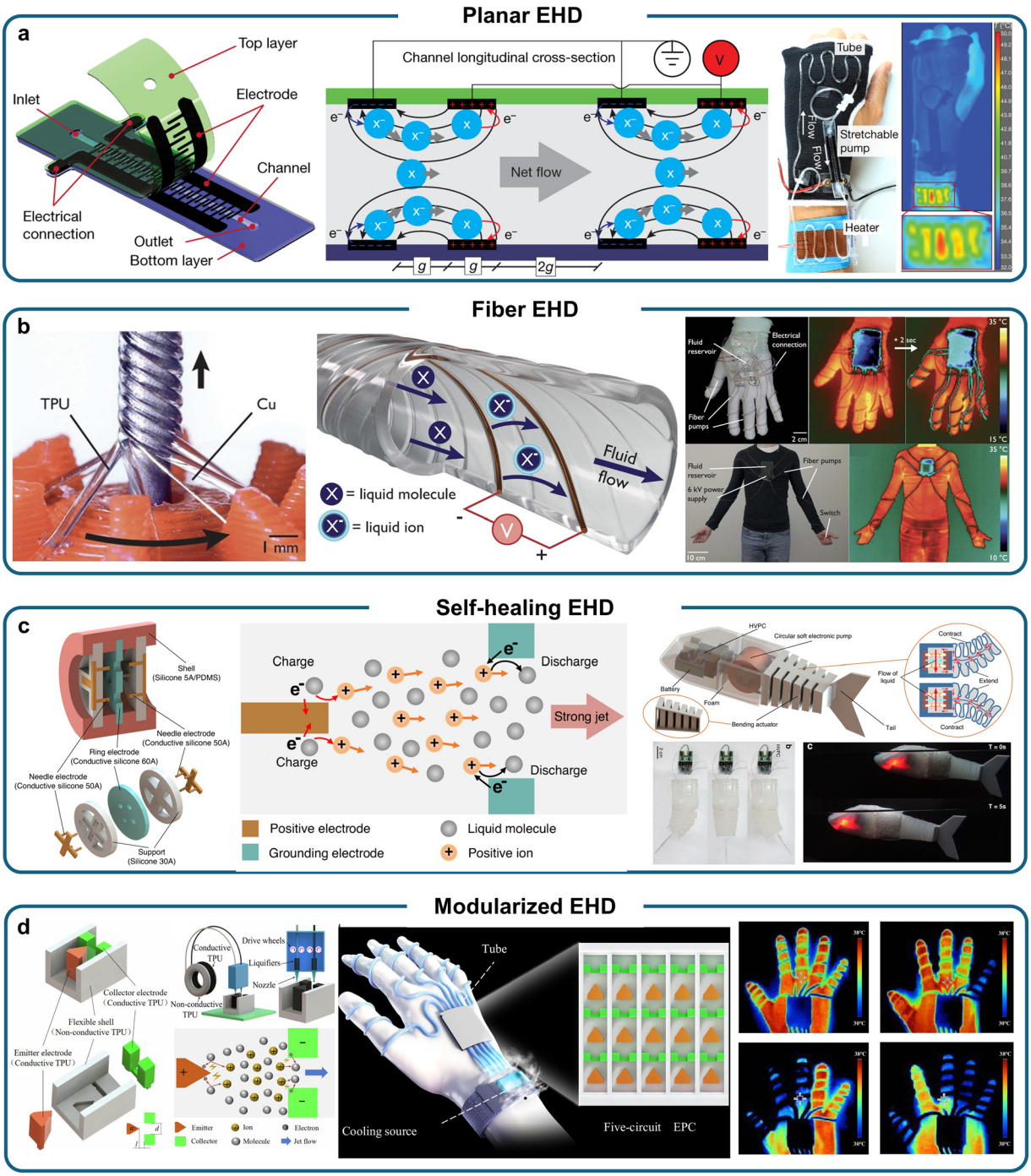

Fig. 5 Electrically driven microfluidic pumps for soft and wearable systems. (a) A stretchable electrohydrodynamic pump with interdigitated electrodes for bidirectional flow control under strain.[46] Reproduced from ref. 46 with permission from Springer Nature, 2019. (b) A fiber-shaped electrohydrodynamic pump with helical electrodes for silent and efficient fluid transport in textiles.[47] Reproduced from ref. 47 with permission from the American Association for the Advancement of Science, 2023. (c) A fully soft, self-healing electrohydrodynamic pump using functional liquids for robust actuation in untethered soft robots.[48] Reproduced from ref. 48 with permission from Springer Nature, 2021. (d) A flexible electrohydraulic power chip with 3D-printed modules for programmable, multi-channel liquid control.[49] Reproduced from ref. 49 with permission from Springer Nature, 2025.

features make them especially suitable for applications requiring compactness, low noise, and a high level of integration, such as miniaturized bioelectronics. Recently, a representative study introduces a fully flexible and stretchable EHD pump based on a charge injection mechanism described in Fig. 5a.[46] The device employs an interdigitated electrode design and is available in two versions: one with silver electrodes formed from patterned silver ink (Ag pump), and the other with carbon electrodes made from a carbon black-elastomer composite (C pump). Both types of electrodes are embedded in PDMS

 This journal is © The Royal Society of Chemistry 2025

Open Access Article. Published on 30 julio 2025. Downloaded on 23/02/2026 2:23:37.
This article is licensed under a Creative Commons Attribution-NonCommercial 3.0 Unported Licence.

elastomer membranes and assembled with a laser-cut fluidic channel layer measuring approximately 55 mm × 2 mm × 0.5 mm, forming a soft sandwich structure. The pump uses fluorinert FC-40 as the working dielectric liquid due to its strong insulation properties and compatibility with PDMS. When a square wave voltage of ±8 kV is applied, the electrodes inject negative charges into the fluid, which drive neutral molecules in the direction of the electric field to produce stable unidirectional flow. Reversing the voltage polarity switches the flow direction. The pump remains operational under strain exceeding 50% and maintains nearly consistent performance at both 0% and 10% strain. Performance testing shows that the two pump types have different advantages. The C pump achieves a maximum flow rate of over 100 μL s^{-1} and generates more than 7 kPa of pressure at +5.6 kV, with a response time of less than 1 second. The flow rate can be modulated by adjusting the applied voltage, and further tailored through modular configurations such as series or parallel operation, offering system-level adaptability to diverse fluidic requirements. It is well suited for applications that demand fast response and high flow rate. The Ag pump, on the other hand, withstands up to +10 kV and delivers a pressure larger than 14 kPa, offering higher pumping capacity and longer operating life. The pump demonstrates versatility across multiple application scenarios. In a wearable thermal regulation glove, the pump circulates fluid in a closed-loop system with a heating membrane and cooling channel. Under a temperature difference of 6 K and a flow rate of 100 μL s^{-1}, the system achieves a heat transfer rate of approximately 1.1 W, while the pump consumes only about 0.1 W, indicating high efficiency and low power consumption. In another example, the pump is integrated into the base of a corrugated soft actuator, driving fluid from a reservoir into an expansion chamber to achieve bending deformation of over 40°, showing promise for use in soft robotics. The pump also supports modular configurations in series or parallel, allowing its pressure or flow output to be tailored to specific requirements for different systems. The flexibility makes it a promising component for closed-loop thermal control systems and distributed fluid handling platforms.

Although EHD pumps based on planar configurations exhibit favorable compliance and actuation performance, their integration into wearable systems, textile-based platforms, or biomimetic muscle structures remains limited due to the inherent constraints of two-dimensional geometries. To address this issue, another study proposed a fiber-shaped EHD pump designed for stretchable and wearable platforms (Fig. 5b).[47] The pump consists of a polyurethane elastomeric tube embedded with two helically wound copper wire electrodes. Fabricated using a filament winding process, the electrodes are partially exposed along the inner wall of the tube, enabling charge injection and fluid actuation. The working fluid, Novec 7100, is a low-conductivity dielectric liquid with a high electrical breakdown strength (~+10 kV mm^{-1}) and excellent electrochemical stability. When a direct current electric field of up to +8 kV mm^{-1} is applied, the fluid near the cathode becomes ionized. The resulting anions migrate toward the anode, dragging neutral molecules to produce a net fluid flow. The asymmetric arrangement of the helical electrodes ensures unidirectional pumping, while reversing the voltage polarity allows for the switching of flow direction. A typical pump configuration (2 mm outer diameter, 1.5 mm inner diameter) achieves pressures over 80 kPa and flow rates tunable from 0 to 55 mL min^{-1} by adjusting the applied voltage and pump length, offering adaptable performance for soft robotic and wearable applications. The corresponding power density reaches 15.2 W kg^{-1}, outperforming most existing flexible pumps for bio-integrated electronics. The pump can operate continuously for over six days without performance degradation, and longer lengths further improve power output per unit mass. In terms of mechanical compliance, the pump maintains stable performance under 15% axial strain. When bent to a radius of 4 mm, the output pressure and flow rate decrease by less than 7% and 12%, respectively. After more than 5000 cycles of repeated stretching and bending, no significant performance degradation is observed. The pump also remains functional under extreme deformations such as coiling and knotting, demonstrating excellent morphological adaptability. This fiber pump can be directly integrated into elastic textiles or flexible structural supports to enable distributed fluid control and localized actuation within soft systems. When combined with non-stretchable fiber-reinforced elastomeric tubing, it forms an inverse hydraulic artificial muscle (IHAM), capable of generating an axial tensile force of approximately 0.5 N under hydraulic actuation, with a frequency response up to 2.4 Hz. Parallel configuration of multiple pumps enhances force output while preserving fast response and low hysteresis characteristics. When woven into fluidic textiles, the pump can generate axial forces up to 1.7 N under structural constraint. The system also supports thermal management functions: multiple independently controlled pumps integrated into wearable components such as gloves enable rapid circulation of coolant, providing spatially and temporally resolved thermal haptic feedback. When extended to full garments, this approach enables active cooling and temperature regulation without external tubing, introducing a novel thermal control capability for wearable electronics.

Beyond the structural variation in device configurations, electric field-driven strategies have also expanded toward new directions in integration with novel functional materials. Fig. 5c presents a fully soft liquid pump featuring autonomous self-healing capability.[48] While maintaining high flexibility, this system introduces a curable self-healing liquid as the working medium, enabling functional recovery after mechanical damage such as punctures or tears. The pump consists entirely of soft components, including needle-shaped positive electrodes, a ring-shaped ground electrode, elastomeric supports, and an outer shell made from conductive silicones and PDMS with varying hardness. The core working fluid is a composite of tung oil and dibutyl

Open Access Article. Published on 30 julio 2025. Downloaded on 23/02/2026 2:23:37.
This article is licensed under a Creative Commons Attribution-NonCommercial 3.0 Unported Licence.

sebacate, which undergoes rapid air-induced solidification to seal damage sites. Experimental results show that the healing time is approximately 6 hours at 35 °C and 24 hours at 24 °C. After healing, the system maintains continuous pumping for over 2 hours without leakage. The self-healed film exhibits strong adhesion to the silicone matrix and retains structural integrity after 200 cycles of 20% strain stretching. The device continues to operate based on the EHD charge-injection mechanism. A strong non-uniform electric field between needle-hole electrode pairs induces electron extraction and ion migration, generating directional fluid flow. The pump comprises multiple symmetric electrode units, enabling bidirectional flow control by selectively activating opposite sets of electrodes rather than reversing voltage polarity. Under ±16 kV square-wave excitation, the system achieves a peak pressure of 9.2 kPa, a frequency response limit of ~10 Hz, and a maximum flow rate of 521 mL min^{-1}. The flow output—tunable up to this maximum—can be programmed by varying fluid composition, electrode geometry (*e.g.*, needle and hole diameters, spacing), and modular pump configuration, allowing structural optimization for diverse application needs. Long-term operation (up to 4 hours) demonstrates stable performance, even with electrode passivation. The performance can be readily tuned through variations in fluid composition, electrode geometry (needle diameter, hole diameter, gap spacing), and modular configuration (series or parallel). Demonstration systems include a soft robotic fish and a robotic vehicle platform. In the fish, the pump drives a bidirectional bending actuator to mimic tail fin motion and enable free swimming underwater. In the vehicle, the pump powers a linear actuator that propels movement under wireless energy transfer, with electromagnetic coils embedded beneath the path. Beyond these specific examples, the pump can serve as a distributed fluidic unit in soft, wearable, or reconfigurable systems, offering robust, self-healing operation for applications such as soft actuators, thermal regulation, and bio-integrated electronics. Building upon the previously reported self-healing flexible EHD pump, the same research team has further advanced a flexible, integrated platform capable of multi-channel liquid manipulation and digital control (Fig. 5d).[49] At its core, the system incorporates flexible electro-hydraulic power chips, which enable independent actuation and programmable switching of multiple fluidic pathways within a single device through modular design, integrated wiring, and high-voltage control. This marks a critical step toward system-level integration and intelligent regulation in electric field-driven fluidic systems. The platform is composed of multiple flexible electrohydraulic "transistor" modules fabricated monolithically *via* multi-material 3D printing of conductive and non-conductive thermoplastic polyurethane. Each module exploits a non-uniform high electric field to inject charges and drive ion migration, thereby producing directional flow of low-conductivity fluids. When operated at +15 kV, a single module achieves a pressure density of up to 10.77 kPa g^{-1} and a flow rate density of 2.15 L min^{-1} g^{-1}, with a response time of approximately 0.67 s and a switching delay of 0.83 s. The output flow rate and pressure can be modulated by adjusting the applied voltage, providing continuous tunability beyond on–off switching. Further control is achieved by selectively activating modules and configuring them in series or parallel, enabling programmable and scalable fluidic performance. Modules can be connected in series or parallel to scale output pressure or flow rate, offering excellent scalability and programmability. This versatile platform demonstrates broad functional adaptability, with use cases spanning wearable fluidic systems and soft robotics. One demonstrated application is a wearable cooling glove, which enables programmable, region-specific thermal regulation of individual fingers through selective fluid delivery—highlighting its practical potential for on-body fluidic manipulation. This work signifies the evolution of flexible electrohydrodynamic systems toward highly integrated, functionally modular, and intelligently controlled architectures, offering standardized, generalizable fluidic actuation solutions for next-generation soft robotics and wearable liquid-handling technologies.

Outlook and future directions

In conclusion, this review summarizes current strategies for liquid transport, with an emphasis on those compatible with integration into bio-integrated electronics in both wearable and implantable formats. Table 1 presents the relevant performance metrics and application contexts of representative, recent works highlighted in this review. It should be noted that, due to varying control mechanisms, device geometries, and application targets, sometimes it is difficult to make direct comparison across different systems using unifying reporting criteria. To address this challenge, Table 2 provides a comparative analysis of four representative liquid transport strategies, each exemplified by a recent study corresponding to a distinct driving mechanism—passive transport, mechanically driven, pressure-mediated, and electric field-driven. These systems are evaluated side-by-side under unified performance metrics, including power consumption, operating voltage, heat generation, transport performance, controllability, bidirectionality, and response speed. This structured comparison offers a practical reference for selecting appropriate fluid handling mechanisms in bio-integrated electronics.

Despite notable progress, several key challenges remain in the following areas (Fig. 6). Further advancement in this field requires the development of systems with miniaturized formats to enhance user comfort and overall device acceptance. This challenge persists because many current liquid transport strategies still depend on relatively bulky actuation components, such as pumps, valves, or reservoirs, to provide sufficient driving force. While existing passive transport strategies—such as those leveraging capillary action, osmotic gradients, or passive flow regulation—can

 This journal is © The Royal Society of Chemistry 2025

Open Access Article. Published on 30 julio 2025. Downloaded on 23/02/2026 2:23:37. This article is licensed under a Creative Commons Attribution-NonCommercial 3.0 Unported Licence.

Table 1 Summary of representative works discussed in this review, key performance metrics, and associated applications

Working principle	Format factors	Power consumption	Transport speed	Applications	Ref.
Passive transport (glandular pressure-driven)	~1 mm thick, 28 mm diameter	None (passive)	~7.8 μL min^{-1}	On-body sweat collection and *in situ* chloride analysis for CF diagnosis	81
Passive transport (capillary and wettability gradient-driven)	~0.65 mm thick, 65 × 30 mm^2 (3D LD substrate)	None (passive)	11.6 mL cm^{-2} min^{-1} (VLD)	Directional, multi-layered sweat transport and sensing for breathable skin-integrated wearables	90
Passive transport (geometry-enabled capillarity)	~32 × 27 × 9 mm^3	None (passive)	N/A	Continuous EBC collection, directional transport, and *in situ* sensing	70
Passive transport (structural asymmetry-induced barrier gradient)	Single fin: 3 × 1.5 × 2 mm^3	None (passive)	~1 mm s^{-1}	Directional liquid transport and switching on structured surfaces	54
Mechanically driven (magnetic field-induced rotation)	36 × 36 × 9 mm^3	4.1 W @ 1000 rpm	30.6 mL min^{-1} @ 1000 rpm	Wearable and implantable fluidic systems for dialysis, blood circulation, and thermal management	29
Mechanically driven (electromagnetic actuation)	~15 × 15 × 10 mm^3	~0.3 W	240 μL min^{-1} @ 180 mA	Multichannel, on-demand delivery of tastants for gustatory interfaces	30
Mechanically driven (electrostatic actuation–induced peristalsis)	~5 × 3 × 2 cm^3	~1.16 W (+1680 V, 200 Hz, single dual-DEA unit)	39 mL min^{-1}	Programmable fluidic actuation for wearable haptic feedback, soft robotic control, and drink mixing	109
Pressure-mediated (electrically induced deformation)	~2 × 1.5 × 0.2 cm^3	0.21 W (+1.8 kV, 7 Hz)	3.25 mL min^{-1} (water), 1.1 mL min^{-1} (ethylene glycol)	Wearable soft fluidic systems for haptic feedback and actuation	114
Pressure-mediated (water electrolysis)	~1.0 × 1.0 × 0.3 cm^3 (pump only)	~3.3 mW @ +3.0 V	Injection: 2.0–3.0 μL min^{-1}; retrieval: ~0.86 μL min^{-1}	Wireless, implantable device for neurochemical sampling in freely moving animals	37
Pressure-mediated (water electrolysis)	~0.7 × 0.9 × 0.6 cm^3 (pump only)	~6 mW @ +3.3 V	~1.15 μL min^{-1}	Wireless, chronic, and dose-controllable drug delivery with simultaneous neural recording in freely behaving mice	38
Pressure-mediated (thermal hydrogel valve)	~4.5 × 7.0 × 0.5 cm^3	~330 mW per valve	N/A (passive gating of sweat flow)	Wireless, time-resolved sweat biomarker analysis *via* programmable sampling and routing	15
Electric field-driven (EHD)	~75 × 19 × 1.3 mm^3	~100 mW	>100 μL s^{-1} (C pump)	Stretchable, bidirectional electrohydrodynamic pump for on-body thermal regulation and untethered soft robotic actuation	46
Electric field-driven (EHD)	2 mm in outer diameter, variable length	~0.9 W @ +8 kV mm^{-1}	Up to 55 mL min^{-1}@ +8 kV mm^{-1}	On-body thermal regulation, haptic feedback, and untethered soft robotic actuation	47
Electric field-driven (EHD)	~24 mm in diameter, 6.8 mm thick	~3.6 W @ +16 kV	Up to 521 mL min^{-1} @ ±16 kV	Wireless, self-healing electrohydrodynamic pump for soft robotics and wearable actuation	48
Electric field-driven (EHD)	~7 × 4 × 3 mm^3	~3.24 W @ +15 kV	Up to 2.15 L min^{-1} g^{-1}@ +15 kV	Modular, multi-channel electrohydrodynamic pump for cooling of wearables and soft robotic control	49

Table 2 Comparative evaluation of liquid transport strategies based on driving mechanisms and key performance metrics

Driving mechanism	Passive transport	Mechanically driven	Pressure-mediated	Electric field-driven
Representative work	Ref. 90	Ref. 29	Ref. 38	Ref. 47
Power consumption	None	High	Low	High
Operating voltage	None	Low	Low	High
Heat generation	None	Medium	Low	Medium
Transport performance	Low	High	Low	High
Flow rate control	No	High	Medium	High
Bidirectional transport capability	No	No	No	Yes
Response speed	High	Medium	Low	High

Open Access Article. Published on 30 julio 2025. Downloaded on 23/02/2026 2:23:37.
This article is licensed under a Creative Commons Attribution-NonCommercial 3.0 Unported Licence.

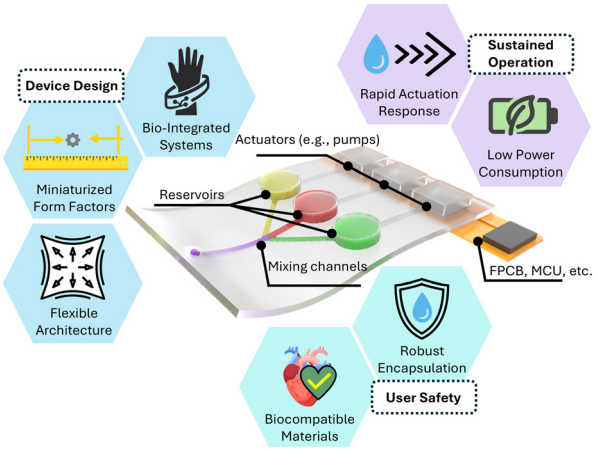

Fig. 6 Outlook and challenges for liquid transport systems in bio-integrated electronics, categorized into three key areas: device design, user safety, and sustained operation.

help circumvent the need for bulky actuation components, they often suffer from limited efficiency and may not be suitable for applications requiring high-speed or high-volume fluid transport. Exploring alternative approaches that emphasize low-profile, energy-efficient actuation mechanisms could potentially address this issue. Options include stimuli-responsive materials—such as hydrogels,[132] shape-memory polymers,[133] and liquid crystal elastomers[134]—that can induce fluid movement without requiring large external hardware. However, although these concepts have been demonstrated in pioneering studies, the feasibility of incorporating them into flexible, bio-integrated electronics remains further exploration.

Among emerging strategies, bioinspired artificial cilia actuators represent a promising but as-yet unproven approach for microfluidic liquid manipulation in wearable and implantable formats. These systems utilize electrochemical surface actuation to induce asymmetric bending and non-reciprocal motion, enabling fluid pumping in low Reynolds number environments without the need for bulky mechanical components or high-power electronics. While these systems have demonstrated precise and programmable fluid control *in vitro*, their application in bio-integrated devices remains largely conceptual. Future translation will require addressing challenges related to biocompatibility, system integration, and long-term stability in physiological environments.

Another critical consideration for on-chip liquid management is power consumption, which directly influences longevity, portability, and feasibility of devices for continuous or long-term use. While sensors are generally designed to operate with low power and can often remain in a standby or low-energy mode, actuators implementing active duties typically require significantly higher power to function. The high energy demands can lead to rapid battery depletion, increased heat generation, and bulky energy storage components, all of which compromise user comfort and system reliability. Typically, there are trade-offs between power consumption, heat generation, response speed, actuation force, and control accuracy. These factors should be carefully considered during the customizable design process. Solutions include developing low-power actuation mechanisms, such as using stimuli-responsive materials discussed above, as well as on-demand or intermittent actuation schemes that reduce the duty cycle and energy usage. The integration of energy harvesting technologies—such as triboelectric,[135] piezoelectric,[136] or thermoelectric[137] generators—offers a promising route to supplement the power supply, which has been discussed elsewhere. For applications where temperature control is critical, it is important to incorporate management units and/or cooling systems to maintain a stable thermal environment.

User safety represents a critical design consideration. In addition to thermal safety, potential hazards may arise from electrical, chemical, and electromagnetic sources. Currently, the diversity of pumping strategies—each differing significantly in design and operation—has led to a lack of consistent reporting standards and benchmarking guidelines for safety evaluation. For applications involving wet or fluidic biological tissues, fully biocompatible encapsulation is essential to prevent corrosion, device malfunction, electric shocks, and chemical leakage. Furthermore, the use of inherently safe and stable materials throughout the system is imperative to ensure long-term reliability and to minimize health risks. Collectively, addressing these issues enables the integration of liquid management strategies into the existing workflow of lab-on-a-chip systems, significantly enhancing their capabilities for the next generation of healthcare platforms featuring automated, programmable, and closed-loop control. These advancements will create fertile ground for the continued development of innovative technologies. While many of the liquid transport strategies discussed in this review have been demonstrated primarily in wearable or externally mounted systems, they also lay essential groundwork for the development of fully implantable platforms. The integration of such systems into long-term, autonomous, and biocompatible implantable devices presents significant challenges—including chronic stability, immune response mitigation, long-duration power supply, and real-time adaptability to physiological environments. Future efforts toward material innovation, energy autonomy, and miniaturized closed-loop control will be critical to enabling reliable liquid handling within the body. As the field progresses, the translation of current strategies into fully implantable formats holds great potential to unlock new applications in precision medicine, continuous monitoring, and targeted therapy.

Another critical and often under-addressed issue concerns the physical integration of liquid transport systems onto or into the human body. In wearable and implantable platforms, the interface between device and tissue must accommodate long-term contact, dynamic motion, sweat, and biological compatibility. Challenges such as mechanical

 This journal is © The Royal Society of Chemistry 2025

Open Access Article. Published on 30 julio 2025. Downloaded on 23/02/2026 2:23:37. This article is licensed under a Creative Commons Attribution-NonCommercial 3.0 Unported Licence.

mismatch, inadequate adhesion, and tissue irritation can lead to signal drift, device detachment, or immune responses. While much of the existing literature focuses on optimizing fluid transport performance, future efforts must also address how these systems are physically anchored to the body, ensuring stable operation and user comfort over extended periods. Effective packaging, soft interfaces, and skin- or tissue-conformal materials will be key enablers in translating fluidic platforms from lab prototypes into real-world, bio-integrated systems. These considerations will be crucial to realizing fluidic systems not only as technological tools, but as viable clinical platforms.

Conflicts of interest

There are no conflicts to declare.

Data availability

No primary research results, software or code have been included and no new data were generated or analysed as part of this review.

Acknowledgements

This work was supported by the National Science Foundation ECCS-2223387; the National Institute Of Biomedical Imaging And Bioengineering of the National Institutes of Health R21EB035153; the Defense Advanced Research Projects Agency HR00112410004; the Chronic Brain Injury Pilot Award Program at The Ohio State University; and the Sloan Research Fellowship.

References

1 G. M. Whitesides, *Nature*, 2006, **442**, 368–373.
2 E. K. Sackmann, A. L. Fulton and D. J. Beebe, *Nature*, 2014, **507**, 181–189.
3 Y. Arango, Y. Temiz, O. Gökçe and E. Delamarche, *Sci. Adv.*, 2020, **6**, eaay8305.
4 P. Azizian, J. Casals–Terré, J. Ricart and J. M. Cabot, *Analyst*, 2023, **148**, 2657–2675.
5 E. Khanjani, A. Fergola, J. A. López Martínez, S. Nazarnezhad, J. Casals Terre, S. L. Marasso and B. Aghajanloo, *Front. Lab Chip Technol.*, 2025, **4**, 1502127.
6 A. P. Iakovlev, A. S. Erofeev and P. V. Gorelkin, *Biosensors*, 2022, **12**, 956.
7 N. Convery and N. Gadegaard, *Micro Nano Eng.*, 2019, **2**, 76–91.
8 M. Cao, Y. Qiu, H. Bai, X. Wang, Z. Li, T. Zhao, Y. Tian, Y. Wu and L. Jiang, *Matter*, 2024, **7**, 3053–3068.
9 Z. Wang, A. K. Mallik, F. Wei, Z. Wang, A. Rout, R. H. Jibon, Q. Wu and Y. Semenova, *Commun. Eng.*, 2024, **3**, 54.
10 B. Aghajanloo, W. Losereewanich, C. J. Pastras and D. W. Inglis, *Biomicrofluidics*, 2024, **18**, 061501.
11 J. Johari, J. Yunas, A. A. Hamzah and B. Y. Majlis, *Sains Malays.*, 2011, **40**, 275–281.
12 O. Français and I. Dufour, *J. Micromech. Microeng.*, 2000, **10**, 282.
13 C. G. Cooney and B. C. Towe, *Sens. Actuators, A*, 2004, **116**, 519–524.
14 J. Yunas, M. M. Said, R. E. Pawinanto, B. Bais, B. Mulyanti, I. Hamidah, A. B. D. Nandiyanto and B. Y. Majlis, *J. Adv. Res. Fluid Mech. Therm. Sci.*, 2021, **85**, 12–21.
15 H. Lin, J. Tan, J. Zhu, S. Lin, Y. Zhao, W. Yu, H. Hojaiji, B. Wang, S. Yang, X. Cheng, Z. Wang, E. Tang, C. Yeung and S. Emaminejad, *Nat. Commun.*, 2020, **11**, 4405.
16 P. H. Lin, H. H. Nien and B. R. Li, *Annu. Rev. Anal. Chem.*, 2023, **16**, 181–203.
17 S. Apoorva, N. T. Nguyen and K. R. Sreejith, *Lab Chip*, 2024, **24**, 1833–1866.
18 C. Wang, T. Zhao, W. Cheng, Z. Ni and N. Xiang, *Device*, 2024, **2**, 100551.
19 Y. Li, C. Xu, Y. Liao, X. Chen, J. Chen, F. Yang and M. Gao, *Biomicrofluidics*, 2024, **18**, 061303.
20 V. Narayanamurthy, Z. Jeroish, K. Bhuvaneshwari, P. Bayat, R. Premkumar, F. Samsuri and M. M. Yusoff, *RSC Adv.*, 2020, **10**, 11652–11680.
21 J. Li and Z. Guo, *Nanoscale*, 2018, **10**, 13814–13831.
22 X. Fu, Y. Qiu, H. Zhang, Y. Tian, A. Liu and H. Wu, *Biomicrofluidics*, 2024, **18**, 034106.
23 P. Sinha Mahapatra, R. Ganguly, A. Ghosh, S. Chatterjee, S. Lowrey, A. D. Sommers and C. M. Megaridis, *Chem. Rev.*, 2022, **122**, 16752–16801.
24 B. Ma, J. Chi, C. Xu, Y. Ni, C. Zhao and H. Liu, *Talanta*, 2020, **212**, 120786.
25 S. Wang, X. Zhang, C. Ma, S. Yan, D. Inglis and S. Feng, *Biosensors*, 2021, **11**, 405.
26 Q. Meng, Z. Li, J. Pang, K. Yang and J. Zhou, *Biomimetics*, 2025, **10**, 223.
27 J. Y. Qian, C. W. Hou, X. J. Li and Z. J. Jin, *Micromachines*, 2020, **11**, 172.
28 U. Roshan, A. Mudugamuwa, H. Cha, S. Hettiarachchi, J. Zhang and N. T. Nguyen, *Lab Chip*, 2024, **24**, 2146–2175.
29 M. Zhou, Z. Qi, Z. Xia, Y. Li, W. Ling, J. Yang, Z. Yang, J. Pei, D. Wu, W. Huo and X. Huang, *Sci. Adv.*, 2021, **7**, eabi7203.
30 S. Chen, Y. Jia, B. Duan, T. L. Liu, Q. Wang, X. Xiao, P. Nithianandam, X. Tian, C. Yang, C. Wu, Z. Xie and J. Li, *Sci. Adv.*, 2025, **11**, eadr4797.
31 W. Wang, Q. Liu, I. Tanasijevic, M. F. Reynolds, A. J. Cortese, M. Z. Miskin, M. C. Cao, D. A. Muller, A. C. Molnar, E. Lauga, P. L. McEuen and I. Cohen, *Nature*, 2022, **605**, 681–686.
32 S. N. Khaderi, C. B. Craus, J. Hussong, N. Schorr, J. Belardi, J. Westerweel, O. Prucker, J. Rühe, J. M. J. den Toonder and P. R. Onck, *Lab Chip*, 2011, **11**, 2002–2010.
33 A. K. Persons, J. E. Ball, C. Freeman, D. M. Macias, C. L. Simpson, B. K. Smith and R. F. V. Burch, *Materials*, 2021, **14**, 4070.
34 R. J. Yang, H. H. Hou, Y. N. Wang and L. M. Fu, *Sens. Actuators, B*, 2016, **224**, 1–15.

Open Access Article. Published on 30 julio 2025. Downloaded on 23/02/2026 2:23:37.
This article is licensed under a Creative Commons Attribution-NonCommercial 3.0 Unported Licence.

35 Y. Lee, F. Koehler, T. Dillon, G. Loke, Y. Kim, J. Marion, M. J. Antonini, I. C. Garwood, A. Sahasrabudhe, K. Nagao, X. Zhao, Y. Fink, E. T. Roche and P. Anikeeva, *Adv. Mater.*, 2023, **35**, 2301916.
36 N. A. Filatov, A. A. Evstrapov and A. S. Bukatin, *Micromachines*, 2021, **12**, 662.
37 G. Wu, I. Heck, N. Zhang, G. Phaup, X. Zhang, Y. Wu, D. E. Stalla, Z. Weng, H. Sun, H. Li, Z. Zhang, S. Ding, D. P. Li and Y. Zhang, *Sci. Adv.*, 2022, **8**, eabn2277.
38 Y. Yoon, H. Shin, D. Byun, J. Woo, Y. Cho, N. Choi and I. J. Cho, *Nat. Commun.*, 2022, **13**, 5521.
39 K. W. Oh, K. Lee, B. Ahn and E. P. Furlani, *Lab Chip*, 2012, **12**, 515–545.
40 F. O. Romero–Soto, L. Weber, D. Mager, M. M. Aeinehvand and S. O. Martinez–Chapa, *Sens. Actuators, B*, 2023, **377**, 133025.
41 V. Miralles, A. Huerre, F. Malloggi and M. C. Jullien, *Diagnostics*, 2013, **3**, 33–67.
42 D. Terutsuki, S. Miyazawa, J. Takagi, A. Yamada, Y. Sun, H. Abe, G. Wang and M. Nishizawa, *Adv. Funct. Mater.*, 2024, **34**, 2304946.
43 J. Tan, Z. Fan, M. Zhou, T. Liu, S. Sun, G. Chen, Y. Song, Z. Wang and D. Jiang, *Adv. Mater.*, 2024, **36**, 2314346.
44 C. T. Ertsgaard, M. Kim, J. Choi and S. H. Oh, *Nat. Commun.*, 2023, **14**, 103.
45 W. Gao, C. Zhang, Y. Cai, F. Su, C. Han, D. Yu, Y. Luo and X. Xing, *Sens. Actuators, B*, 2024, **410**, 135669.
46 V. Cacucciolo, J. Shintake, Y. Kuwajima, S. Maeda, D. Floreano and H. Shea, *Nature*, 2019, **572**, 516–519.
47 M. Smith, V. Cacucciolo and H. Shea, *Science*, 2023, **379**, 1327–1332.
48 W. Tang, C. Zhang, Y. Zhong, P. Zhu, Y. Hu, Z. Jiao, X. Wei, G. Lu, J. Wang, Y. Liang, Y. Lin, W. Wang, H. Yang and J. Zou, *Nat. Commun.*, 2021, **12**, 2247.
49 S. Zheng, X. M. Zhang, H. S. Liu, G. H. Liang, S. W. Zhang, W. Zhang, B. Wang, J. Yang, X. Jin, F. Pan and J. F. Li, *Nat. Commun.*, 2025, **16**, 1–13.
50 Y. Peng, D. Li, X. Yang, Z. Ma and Z. Mao, *Micromachines*, 2023, **14**, 321.
51 Z. Mao, N. Hosoya and S. Maeda, *Cyborg Bionic Syst.*, 2024, **5**, 0091.
52 Y. Kuwajima, A. Marzuq, S. Segawa, Y. Yamaguchi, Y. Yamada, T. Morita, K. Morozov, H. Iwasaki, S. Suzuki, H. Nabae, V. Cacucciolo, N. Hosoya, Y. Kakehi and S. Maeda, *Adv. Sci.*, 2025, **12**, e2416502.
53 Z. Mao, T. Iizuka and S. Maeda, *Sens. Actuators, A*, 2021, **332**, 113168.
54 L. Yang, W. Li, J. Lian, H. Zhu, Q. Deng, Y. Zhang, J. Li, X. Yin and L. Wang, *Science*, 2024, **384**, 1344–1349.
55 M. Yafia, O. Ymbern, A. O. Olanrewaju, A. Parandakh, A. Sohrabi Kashani, J. Renault, Z. Jin, G. Kim, A. Ng and D. Juncker, *Nature*, 2022, **605**, 464–469.
56 R. F. R. Ursem, A. Steijlen, M. Parrilla, J. Bastemeijer, A. Bossche and K. De Wael, *Lab Chip*, 2025, **25**, 1296–1315.
57 L. B. Baker, *Sports Med.*, 2017, **47**, 111–128.
58 J. Brunmair, M. Gotsmy, L. Niederstaetter, B. Neuditschko, A. Bileck, A. Slany, M. L. Feuerstein, C. Langbauer, L. Janker, J. Zanghellini, S. M. Meier-Menches and C. Gerner, *Nat. Commun.*, 2021, **12**, 5993.
59 J. Min, J. R. Sempionatto, H. Teymourian, J. Wang and W. Gao, *Biosens. Bioelectron.*, 2021, **172**, 112750.
60 B. Jagannath, M. Pali, K. C. Lin, D. Sankhala, P. Naraghi, S. Muthukumar and S. Prasad, *Adv. Mater. Technol.*, 2022, **7**, 2101356.
61 A. Koh, D. Kang, Y. Xue, S. Lee, R. M. Pielak, J. Kim, T. Hwang, S. Min, A. Banks, P. Bastien, M. C. Manco, L. Wang, K. R. Ammann, K. I. Jang, P. Won, S. Han, R. Ghaffari, U. Paik, M. J. Slepian, G. Balooch, Y. Huang and J. A. Rogers, *Sci. Transl. Med.*, 2016, **8**, 366ra165.
62 J. T. Reeder, Y. Xue, D. Franklin, Y. Deng, J. Choi, O. Prado, R. Kim, C. Liu, J. Hanson, J. Ciraldo, A. J. Bandodkar, S. Krishnan, A. Johnson, E. Patnaude, R. Avila, Y. Huang and J. A. Rogers, *Nat. Commun.*, 2019, **10**, 5513.
63 L. B. Baker, J. B. Model, K. A. Barnes, M. L. Anderson, S. P. Lee, K. A. Lee, S. D. Brown, A. J. Reimel, T. J. Roberts, R. P. Nuccio, J. L. Bonsignore, C. T. Ungaro, J. M. Carter, W. Li, M. S. Seib, J. T. Reeder, A. J. Aranyosi, J. A. Rogers and R. Ghaffari, *Sci. Adv.*, 2020, **6**, eabe3929.
64 F. Gao, C. Liu, L. Zhang, T. Liu, Z. Wang, Z. Song, H. Cai, Z. Fang, J. Chen, J. B. Wang, M. Han, J. Wang, K. Lin, R. Wang, M. Li, Q. Mei, X. Ma, S. Liang, G. Gou and N. Xue, *Microsyst. Nanoeng.*, 2023, **9**, 1.
65 Y. Zhang, H. Guo, S. B. Kim, Y. Wu, D. Ostojich, S. H. Park, X. Wang, Z. Weng, R. Li, A. J. Bandodkar, Y. Sekine, J. Choi, S. Xu, S. Quaggin, R. Ghaffari and J. A. Rogers, *Lab Chip*, 2019, **19**, 1545–1555.
66 J. T. Reeder, J. Choi, Y. Xue, P. Gutruf, J. Hanson, M. Liu, T. Ray, A. J. Bandodkar, R. Avila, W. Xia, S. Krishnan, S. Xu, K. Barnes, M. Pahnke, R. Ghaffari, Y. Huang and J. A. Rogers, *Sci. Adv.*, 2019, **5**, eaau6356.
67 A. J. Bandodkar, W. J. Jeang, R. Ghaffari and J. A. Rogers, *Annu. Rev. Anal. Chem.*, 2019, **12**, 1–22.
68 X. M. Chen, Y. J. Li, D. Han, H. C. Zhu, C. D. Xue, H. C. Chui, T. Cao and K. R. Qin, *Micromachines*, 2019, **10**, 457.
69 Y. Wang, L. Yin, Y. Bai, S. Liu, L. Wang, Y. Zhou, C. Hou, Z. Yang, H. Wu, J. Ma, Y. Shen, P. Deng, S. Zhang, T. Duan, Z. Li, J. Ren, L. Xiao, Z. Yin, N. Lu and Y. Huang, *Sci. Adv.*, 2020, **6**, eabd0996.
70 W. Heng, S. Yin, J. Min, C. Wang, H. Han, E. Shirzaei Sani, J. Li, Y. Song, H. B. Rossiter and W. Gao, *Science*, 2024, **385**, 954–961.
71 Z. Wang, Y. Dong, X. Sui, X. Shao, K. Li, H. Zhang, Z. Xu and D. Zhang, *npj Flexible Electron.*, 2024, **8**, 35.
72 R. Moreddu, M. Elsherif, H. Adams, D. Moschou, M. F. Cordeiro, J. S. Wolffsohn, D. Vigolo, H. Butt, J. M. Cooper and A. K. Yetisen, *Lab Chip*, 2020, **20**, 3970–3979.2.
73 H. Su, F. Sun, Z. Lu, J. Zhang, W. Zhang and J. Liu, *Sens. Actuators, B*, 2022, **357**, 131459.
74 R. Liu, Q. Nie, Y. Wang, Y. Wu, Y. Tu, C. Xie, X. Xiao, R. You and Y. Lu, *Chem. Eng. J.*, 2024, **498**, 155207.
75 X. Yang, O. Forouzan, T. P. Brown and S. S. Shevkoplyas, *Lab Chip*, 2012, **12**, 274–280.

 This journal is © The Royal Society of Chemistry 2025

Open Access Article. Published on 30 julio 2025. Downloaded on 23/02/2026 2:23:37. This article is licensed under a Creative Commons Attribution-NonCommercial 3.0 Unported Licence.

76 T. Songjaroen, W. Dungchai, O. Chailapakul, C. S. Henry and W. Laiwattanapaisal, *Lab Chip*, 2012, **12**, 3392–3398.
77 J. Kim, G. Valdés-Ramírez, A. J. Bandodkar, W. Jia, A. G. Martinez, J. Ramírez, P. Mercier and J. Wang, *Analyst*, 2014, **139**, 1632–1636.
78 J. Kim, S. Imani, W. R. de Araujo, J. Warchall, G. Valdés-Ramírez, T. R. Paixão, P. P. Mercier and J. Wang, *Biosens. Bioelectron.*, 2015, **74**, 1061–1068.
79 C. Wang, K. Fan, E. Shirzaei Sani, J. A. Lasalde-Ramírez, W. Heng, J. Min, S. A. Solomon, M. Wang, J. Li, H. Han, G. Kim, S. Shin, A. Seder, C.-D. Shih, D. G. Armstrong and W. Gao, *Sci. Transl. Med.*, 2025, **17**, eadt0882.
80 I. Shitanda, Y. Fujimura, T. Takarada, R. Suzuki, T. Aikawa, M. Itagaki and S. Tsujimura, *ACS Sens.*, 2021, **6**, 3409–3415.
81 T. R. Ray, M. Ivanovic, P. M. Curtis, D. Franklin, K. Guventurk, W. J. Jeang, J. Chafetz, H. Gaertner, G. Young, S. Rebollo, J. B. Model, S. P. Lee, J. Ciraldo, J. T. Reeder, A. Hourlier-Fargette, A. J. Bandodkar, J. Choi, A. J. Aranyosi, R. Ghaffari, S. A. McColley, S. Haymond and J. A. Rogers, *Sci. Transl. Med.*, 2021, **13**, eabd8109.
82 A. Nilghaz, D. R. Ballerini and W. Shen, *Biomicrofluidics*, 2013, **7**, 051501.
83 I. Öberg Månsson, A. Piper and M. M. Hamedi, *Macromol. Biosci.*, 2020, **20**, 2000150.
84 M. Hanze, A. Piper and M. M. Hamedi, *Lab Chip*, 2025, **25**, 28–40.
85 Z. Zhao, Q. Li, L. Chen, Y. Zhao, J. Gong, Z. Li and J. Zhang, *Lab Chip*, 2021, **21**, 916–932.
86 L. Lao, D. Shou, Y. S. Wu and J. T. Fan, *Sci. Adv.*, 2020, **6**, eaaz0013.
87 X. He, S. Yang, Q. Pei, Y. Song, C. Liu, T. Xu and X. Zhang, *ACS Sens.*, 2020, **5**, 1548–1554.
88 M. Galliani, E. Ismailova, P. Azizian, A. Makhinia and J. M. Cabot, *npj Flexible Electron.*, 2025, **9**, 38.
89 A. Childs, B. Mayol, J. A. Lasalde–Ramírez, Y. Song, J. R. Sempionatto and W. Gao, *ACS Nano*, 2024, **18**, 24605–24616.
90 B. Zhang, J. Li, J. Zhou, L. Chow, G. Zhao, Y. Huang, Z. Ma, Q. Zhang, Y. Yang, C. K. Yiu, J. Li, F. Chun, X. Huang, Y. Gao, P. Wu, S. Jia, H. Li, D. Li, Y. Liu, K. Yao, R. Shi, Z. Chen, B. L. Khoo, W. Yang, F. Wang, Z. Zheng, Z. Wang and X. Yu, *Nature*, 2024, **628**, 84–92.
91 I. Horváth, J. Hunt and P. J. Barnes, ATS/ERS Task Force on Exhaled Breath Condensate, *Eur. Respir. J.*, 2005, **26**, 523–548.
92 W. Ibrahim, M. J. Wilde, R. L. Cordell, M. Richardson, D. Salman, R. C. Free, B. Zhao, A. Singapuri, B. Hargadon, E. A. Gaillard, T. Suzuki, L. L. Ng, T. Coats, P. Thomas, P. S. Monks, C. E. Brightling, N. J. Greening and S. Siddiqui, the EMBER Consortium, *Sci. Transl. Med.*, 2022, **14**, eabl5849.
93 J. Hunt, *J. Allergy Clin. Immunol.*, 2002, **110**, 28–34.
94 P. Kubáň and F. Foret, *Anal. Chim. Acta*, 2013, **805**, 1–18.
95 N. Hashemzadeh, E. Rahimpour and A. Jouyban, *J. Pharm. Pharm. Sci.*, 2023, **26**, 12042.
96 X. Liu and B. Hu, *Anal. Bioanal. Chem.*, 2023, **415**, 3759–3768.
97 D. Maier, E. Laubender, A. Basavanna, S. Schumann, F. Güder, G. A. Urban and C. Dincer, *ACS Sens.*, 2019, **4**, 2945–2951.
98 Y. Cui, D. Li and H. Bai, *Ind. Eng. Chem. Res.*, 2017, **56**, 4887–4897.
99 B. Chen, Z. Qian, G. Song, X. Niu, Y. Yu, S. Wang, J. Wu, S. Ma, Y. Liang and L. Ren, *Nano Lett.*, 2025, **25**, 3817–3825.
100 K. A. Gopinathan, A. Mishra, B. R. Mutlu, J. F. Edd and M. Toner, *Nature*, 2023, **622**, 735–741.
101 D. C. Leslie, C. J. Easley, E. Seker, J. M. Karlinsey, M. Utz, M. R. Begley and J. P. Landers, *Nat. Phys.*, 2009, **5**, 231–235.
102 B. Li, L. Zhang, S. Bai, J. Jin and H. Chen, *Biomicrofluidics*, 2024, **18**, 021506.
103 Q. Yan, Z. Liu, L. Wang, W. Sun and M. Jiang, *Micromachines*, 2025, **16**, 474.
104 W. Hilber, *Appl. Phys. A: Mater. Sci. Process.*, 2016, **122**, 751.
105 Y. Liu, W. Park, C. K. Yiu, X. Huang, S. Jia, Y. Chen, H. Zhang, H. Chen, P. Wu, M. Wu, Z. Liu, Y. Gao, K. Zhu, Z. Zhao, Y. Li, T. Yokota, T. Someya and X. Yu, *Proc. Natl. Acad. Sci. U. S. A.*, 2024, **121**, e2412116121.
106 H. Miyashita, Proc. ACM UIST, 2021, UIST '21, 37–40.
107 H. Miyashita, Proc. ACM UIST, 2020, UIST '20, 1085–1093.
108 K. W. Song, S. T. Tung, A. Kim and E. Paulos, Proc. ACM UIST, 2024, CHI '24.
109 S. Xu, C. M. Nunez, M. Souri and R. J. Wood, *Sci. Robot.*, 2023, **8**, eadd4649.
110 W. Wu, *Analyst*, 2018, **143**, 4819–4835.
111 X. Luo, L. Yang and Y. Cui, *Sens. Actuators, A*, 2023, **363**, 114732.
112 I. V. Uvarov, P. S. Shlepakov, A. E. Melenev, K. Ma, V. B. Svetovoy and G. J. Krijnen, *Actuators*, 2021, **10**, 62.
113 J. Xie, Y. Miao, J. Shih, Q. He, J. Liu, Y. C. Tai and T. D. Lee, *Anal. Chem.*, 2004, **76**, 3756–3763.
114 L. Wang, J. Zhuo, J. Peng, H. Dong, S. Jiang and Y. Shi, *Adv. Funct. Mater.*, 2024, **34**, 2411160.
115 H. Joo, Y. Lee, J. Kim, J. S. Yoo, S. Yoo, S. Kim, A. K. Arya, S. Kim, S. H. Choi, N. Lu, H. S. Lee, S. Kim, S. T. Lee and D. H. Kim, *Sci. Adv.*, 2021, **7**, eabd4639.
116 V. Iacovacci, I. Tamadon, E. F. Kauffmann, S. Pane, V. Simoni, L. Marziale, M. Aragona, L. Cobuccio, M. Chiarugi, P. Dario, S. Del Prato, L. Ricotti, F. Vistoli and A. Menciassi, *Sci. Robot.*, 2021, **6**, eabh3328.
117 J. Koo, S. B. Kim, Y. S. Choi, Z. Xie, A. J. Bandodkar, J. Khalifeh, Y. Yan, H. Kim, M. K. Pezhouh, K. Doty, G. Lee, Y. Y. Chen, S. M. Lee, D. D'Andrea, K. Jung, K. H. Lee, K. Li, S. Jo, H. Wang, J. H. Kim, J. Kim, S. G. Choi, W. J. Jang, Y. S. Oh, I. Park, S. S. Kwak, J. H. Park, D. Hong, X. Feng, C. H. Lee, A. Banks, C. Leal, H. M. Lee, Y. Huang, C. K. Franz, W. Z. Ray, M. MacEwan, S. K. Kang and J. A. Rogers, *Sci. Adv.*, 2020, **6**, eabb1093.
118 W. Whyte, D. Goswami, S. X. Wang, Y. Fan, N. A. Ward, R. E. Levey, R. Beatty, S. T. Robinson, D. Sheppard, R. O'Connor, D. S. Monahan, L. Trask, K. L. Mendez, C. E.

Open Access Article. Published on 30 julio 2025. Downloaded on 23/02/2026 2:23:37.
This article is licensed under a Creative Commons Attribution-NonCommercial 3.0 Unported Licence.

Varela, M. A. Horvath, R. Wylie, J. O'Dwyer, D. A. Domingo-Lopez, A. S. Rothman, G. P. Duffy, E. B. Dolan and E. T. Roche, *Nat. Commun.*, 2022, **13**, 4496.

119 R. Qazi, A. M. Gomez, D. C. Castro, Z. Zou, J. Y. Sim, Y. Xiong, J. Abdo, C. Y. Kim, A. Anderson, F. Lohner, S. H. Byun, B. C. Lee, K. I. Jang, J. Xiao, M. R. Bruchas and J. W. Jeong, *Nat. Biomed. Eng.*, 2019, **3**, 655–669.

120 E. Meng and T. Hoang, *Adv. Drug Delivery Rev.*, 2012, **64**, 1628–1638.

121 Y. Wu, M. Wu, A. Vázquez-Guardado, J. Kim, X. Zhang, R. Avila, J. T. Kim, Y. Deng, Y. Yu, S. Melzer, Y. Bai, H. Yoon, L. Meng, Y. Zhang, H. Guo, L. Hong, E. E. Kanatzidis, C. R. Haney, E. A. Waters, A. R. Banks, Z. Hu, F. Lie, L. P. Chamorro, B. L. Sabatini, Y. Huang, Y. Kozorovitskiy and J. A. Rogers, *Nat. Commun.*, 2022, **13**, 5571.

122 Y. Zhang, D. C. Castro, Y. Han, Y. Wu, H. Guo, Z. Weng, Y. Xue, J. Ausra, X. Wang, R. Li, G. Wu, A. Vázquez-Guardado, Y. Xie, Z. Xie, D. Ostojich, D. Peng, R. Sun, B. Wang, Y. Yu, J. P. Leshock, S. Qu, C. J. Su, W. Shen, T. Hang, A. Banks, Y. Huang, J. Radulovic, P. Gutruf, M. R. Bruchas and J. A. Rogers, *Proc. Natl. Acad. Sci. U. S. A.*, 2019, **116**, 21427–21437.

123 R. Avila, C. Li, Y. Xue, J. A. Rogers and Y. Huang, *Proc. Natl. Acad. Sci. U. S. A.*, 2021, **118**, e2026405118.

124 R. Avila, Y. Wu, J. A. Rogers and Y. Huang, *J. Mech. Phys. Solids*, 2021, **156**, 104622.

125 D. J. Beebe, J. S. Moore, J. M. Bauer, Q. Yu, R. H. Liu, C. Devadoss and B. H. Jo, *Nature*, 2000, **404**, 588–590.

126 K. Brower, R. R. Puccinelli, C. J. Markin, T. C. Shimko, S. A. Longwell, B. Cruz, R. Gomez–Sjoberg and P. M. Fordyce, *HardwareX*, 2018, **3**, 117–134.

127 C. F. Chen, J. Liu, C. C. Chang and D. L. DeVoe, *Lab Chip*, 2009, **9**, 3511–3516.

128 K. Iranshahi, T. Defraeye, R. M. Rossi and U. C. Müller, *Int. J. Heat Mass Transfer*, 2024, **232**, 125895.

129 D. L. Chen, C. T. Zhou, Y. Zhang, K. Luo and H. L. Yi, *Acta Mech. Sin.*, 2024, **40**, 223115.

130 F. Li, S. Sun, X. Wan, M. Sun, S. L. Zhang and M. Xu, *Nat. Commun.*, 2025, **16**, 1315.

131 Y. Xin, X. Zhou, M. R. J. Tan, S. Chen, P. Huang, Y. Jiang, W. Wu, D. Gao, J. Lv, S. Magdassi and P. S. Lee, *Adv. Mater.*, 2025, **37**, e2415210.

132 G. Graeber, C. D. Díaz–Marín, L. C. Gaugler and B. El Fil, *Nano Lett.*, 2024, **24**, 3858–3865.

133 W. Q. Ye, X. P. Liu, R. F. Ma, C. G. Yang and Z. R. Xu, *Lab Chip*, 2023, **23**, 2068–2074.

134 D. Ditter, P. Blümler, B. Klöckner, J. Hilgert and R. Zentel, *Adv. Funct. Mater.*, 2019, **29**, 1902454.

135 W. Xu, H. Zheng, Y. Liu, X. Zhou, C. Zhang, Y. Song, X. Deng, M. Leung, Z. Yang, R. X. Xu, Z. L. Wang, X. C. Zeng and Z. Wang, *Nature*, 2020, **578**, 392–396.

136 X. Wang, J. Song, J. Liu and Z. L. Wang, *Science*, 2007, **316**, 102–105.

137 A. Sakai, S. Minami, T. Koretsune, T. Chen, T. Higo, Y. Wang, T. Nomoto, M. Hirayama, S. Miwa, D. Nishio-Hamane, F. Ishii, R. Arita and S. Nakatsuji, *Nature*, 2020, **581**, 53–57.

 This journal is © The Royal Society of Chemistry 2025